BIO-RENEWABLE SUPERCAPACITOR WITH IMPROVED PERFORMANCE BASED ON RICE WASTES-DERIVED CARBON DOTS AND ACTIVATED CARBON AND RICE-BASED ELECTROLYTE

BY

MR THANAPAT JORN-AM

A THESIS SUBMITTED IN PARTIAL FULFILLMENT OF
THE REQUIREMENTS FOR THE DEGREE OF
MASTER OF SCIENCE (CHEMISTRY)
DEPARTMENT OF CHEMISTRY
FACULTY OF SCIENCE AND TECHNOLOGY
THAMMASAT UNIVERSITY
ACADEMIC YEAR 2020
COPYRIGHT OF THAMMASAT UNIVERSITY

BIO-RENEWABLE SUPERCAPACITOR WITH IMPROVED PERFORMANCE BASED ON RICE WASTES-DERIVED CARBON DOTS AND ACTIVATED CARBON AND RICE-BASED ELECTROLYTE

BY

MR THANAPAT JORN-AM

A THESIS SUBMITTED IN PARTIAL FULFILLMENT OF
THE REQUIREMENTS FOR THE DEGREE OF
MASTER OF SCIENCE (CHEMISTRY)
DEPARTMENT OF CHEMISTRY
FACULTY OF SCIENCE AND TECHNOLOGY
THAMMASAT UNIVERSITY
ACADEMIC YEAR 2020
COPYRIGHT OF THAMMASAT UNIVERSITY

THAMMASAT UNIVERSITY

FACULTY OF SCIENCE AND TECHNOLOGY
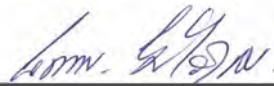
THESIS

BY

MR THANAPAT JORN-AM

ENTITLED

BIO-RENEWABLE SUPERCAPACITOR WITH IMPROVED PERFORMANCE
BASED ON RICE WASTES-DERIVED CARBON DOTS AND ACTIVATED
CARBON AND RICE-BASED ELECTROLYTE

was approved as partial fulfillment of the requirements for

the degree of Master of Science (Chemistry)

on July 14 , 2021

Chairman _____

(Associate Professor Napaporn Youngvises, Ph.D.)
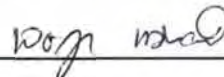
Member and Advisor _____

(Associate Professor Peerasak Paoprasert, Ph.D.)

Member _____

(Assistant Professor Torsak Luanphaisarnnont, Ph.D.)

Member _____

(Jedsada Manyam, Ph.D.)

Dean _____

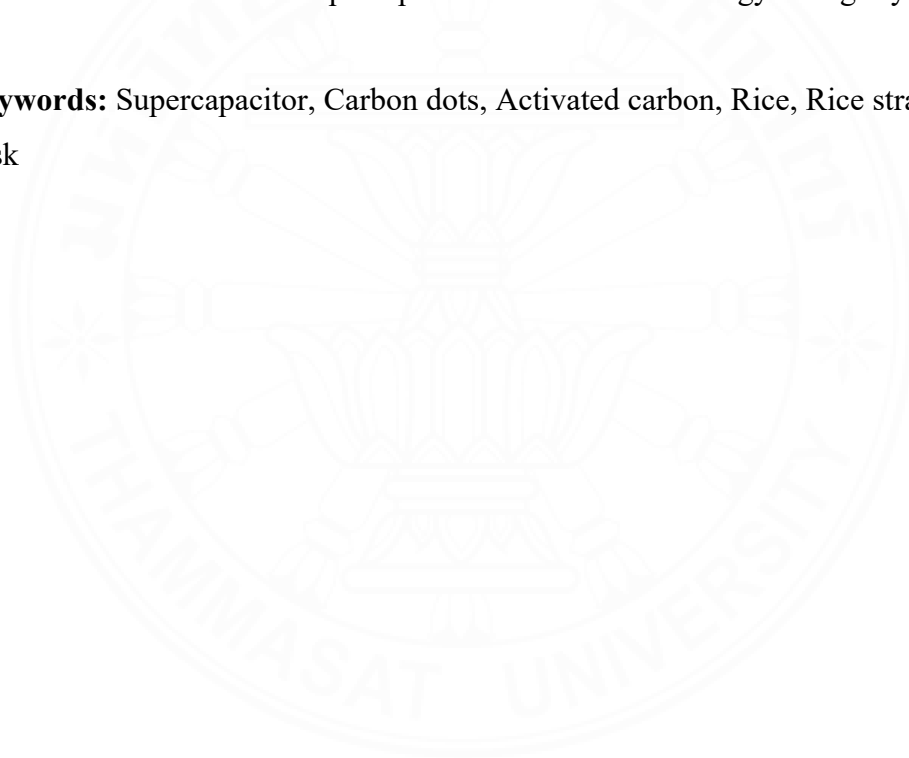(Associate Professor Nuttanont Hongwarittorrn, Ph.D.)

Thesis Title	BIO-RENEWABLE SUPERCAPACITOR WITH IMPROVED PERFORMANCE BASED ON RICE WASTES-DERIVED CARBON DOTS AND ACTIVATED CARBON AND RICE-BASED ELECTROLYTE
Author	Mr Thanapat Jorn-am
Degree	Master of Science (Chemistry)
Department/Faculty/University	Department of Chemistry Faculty of Science and Technology Thammasat University
Thesis Advisor	Associate Professor Peerasak Paoprasert, Ph.D.
Academic Year	2020

ABSTRACT

A high-performance energy storage device fabricated from readily available, abundant resources is highly desirable for large-scale and low-cost electronic applications. In this work, an environmentally friendly carbohydrate-based supercapacitor with a high energy density was developed from bio-renewable rice and rice wastes. Specifically, both activated carbon and carbon dots were prepared together from rice straw and rice husk. The obtained activated carbon was used to make an electrode while the carbon dots were combined with (i) bio-renewable rice for the preparation of electrolytes and (ii) activated carbon for the preparation of CDs-reinforce activated carbon electrode. The fabricated supercapacitor using rice straw-derived activated carbon (RSAC) in rice electrolyte yielded a specific capacitance, potential window, and energy density of 88 F g^{-1}, 2 V, and 12 Wh kg^{-1}, respectively, at a scan rate of 30 mV s^{-1}. For the first time in supercapacitor, the addition of rice straw carbon dots (RSCDs) to rice electrolytes further increased the specific capacitance, potential window, and energy density are 144 F g^{-1}, 2.4 V, and 29 Wh kg^{-1}, equivalent to 163, 120, and 241% increases, respectively, at the same scan rate. The highest specific capacitance and energy density obtained in this work were 491 F g^{-1} and 98 Wh kg^{-1} at

a scan rate of 2 mV s^{-1}. As a comparison, electrolyte prepared from a conventional poly(vinyl alcohol) yielded only 45 F g^{-1}, 1.6 V, and 4 Wh kg^{-1}. The rice husk-derived activated carbon (RHAC) and carbon dots (RHCDs) were used to fabricate CDs-reinforce activated carbon electrode. The RHAC/RHCDs electrode displayed a higher specific capacitance of 129 F g^{-1} and energy density of 4.8 Wh kg^{-1} when compared with those of the bare AC electrode (specific capacitance of 104 F g^{-1} and energy density of 3.6 Wh kg^{-1}). The addition of RHCDs increased the specific capacitance and energy density by 124 and 133%, respectively. This work can also be applied to other abundant biomasses, which will increase their value by using them in the high-performance and low-cost supercapacitor as an efficient energy storage system.

ACKNOWLEDGEMENTS

TABLE OF CONTENTS

LIST OF TABLES

LIST OF FIGURES

LIST OF ABBREVIATIONS

Symbols/Abbreviations	Terms
%w/w	Percent weight by weight
%wt	Weight percent
°C	Degree Celsius
A g^{-1}	Ampere per gram
AC	Activated carbon
Ag	Silver
AgCl	Silver chloride
BET	Brunauer-Emmett- Teller
BJH	Barret-Joner-Halenda
CB	Carbon black
CDs	Carbon dots
cm^{-1}	Per centimeter
cm^3 g^{-1}	Cubic centimeter per gram
C$_{sp}$	Specific capacitance
CV	Cyclic voltammetry
E	Energy density
EDLC	Electric double-layer capacitor
EIS	Electrochemical impedance spectroscopy
eV	Electron volt
F g^{-1}	Farad per pram
FT-IR	Fourier transform infrared spectroscopy
g	Gram
GCD	Galvanostatic charge-discharge
h	Hour
H$_3$PO$_4$	Phosphoric acid
HNO$_3$	Nitric acid
HSC	Hybrid capacitor

Symbols/Abbreviations	Terms
IR	Internal resistance
KBr	Potassium bromide
kDA	Kilodaltons
KOH	Potassium hydroxide
M	Molar
$m^2\ g^{-1}$	Square meter per gram
mA	Milliampere
mg	Milligram
min	Minute
mL	Milliliter
mV	Millivolt
$mV\ s^{-1}$	Millivolt per second
MWCO	Molecular weight cut off
N_2	Nitrogen gas
NaOH	Sodium hydroxide
nm	Nanometer
NMP	N-Methyl-2-pyrrolidone
P	Power density
PC	Pseudocapacitor
pH	Potential of hydrogen ion
Pt	Platinum
PVA	Polyvinyl alcohol
PVDF	Polyvinylidene fluoride
R^2	Coefficients of determination
RHAC	Rice husk activated carbon
RHCDs	Rice husk carbon dots
RSAC	Rice straw activated carbon
RSCDs	Rice straw carbon dots
SEM	Scanning electron microscope

Symbols/Abbreviations	Terms
TEM	Transmission electron microscope
UV	Ultraviolet
V	Volt
Wh kg^{-1}	Watt-hour per kilogram
XPS	X-ray photoelectron spectroscopy
μm	Micrometer
Ω	Ohm
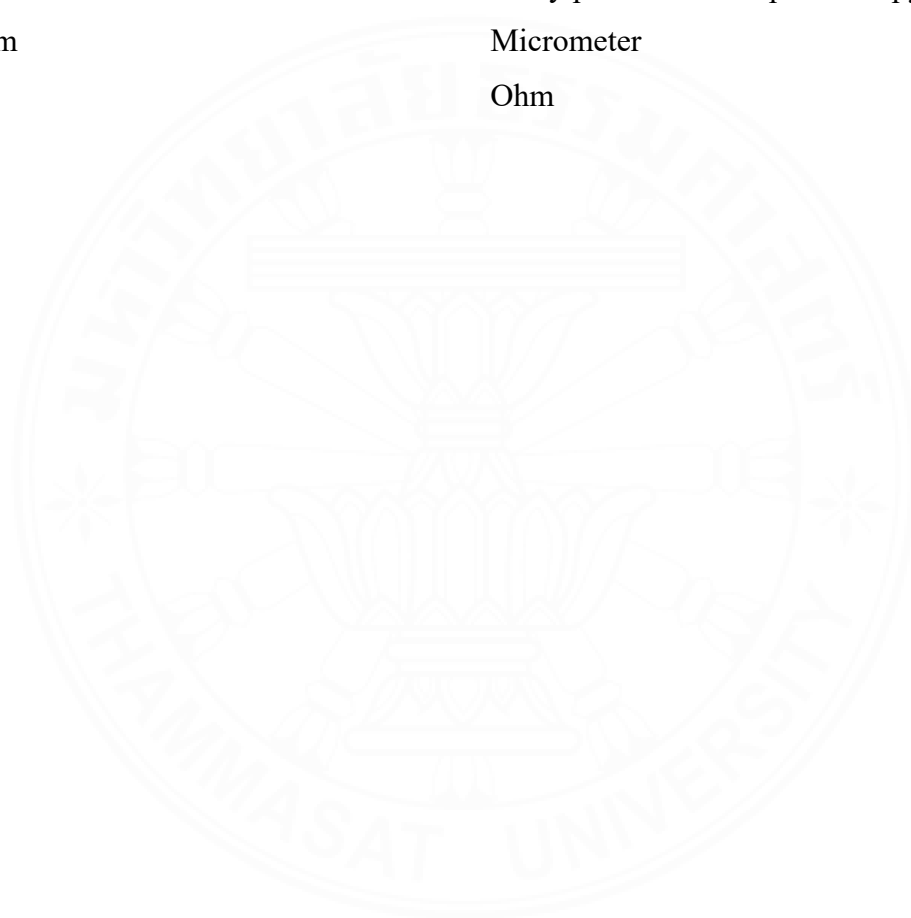
CHAPTER 1

INTRODUCTION

1.1 Problem statement

The supercapacitor is an interesting energy storage device with high power density, fast charge-discharge rate, high stability, and long-cycle life. However, the limitation of supercapacitor is low energy density. (Zhang et al., 2019) In addition, normally supercapacitors are liquid-based electrolytes, which have disadvantages like leakage and erosion caused by liquid electrolytes. (Zhong et al., 2015) Thus, solving these problems will lead to high energy density, long-lasting supercapacitor.

The problem of the low energy density of supercapacitors can be improved by using high specific capacitance materials as electrodes, such as highly porous activated carbon. Moreover, this problem can be alleviated by achieving a wide potential window using suitable electrolytes. Both high specific capacitance materials and high voltage window electrolytes are thus simultaneously contributed to the improvement in energy density. Leakage and erosion of supercapacitors are also important issues. Most reported liquid electrolytes are based on acid solutions, which are corrosive. They shorten the cycle life of the supercapacitors. Recently, Moshuqi Zhu et al. prepared a cellulose-based ion gel polymer electrolyte (Zhu et al., 2019) without the use of acids and achieved good capacity retention and charge-discharge efficiency. This work indicates the attractiveness of polymer-based electrolytes.

1.2 Research objectives

1.2.1 To synthesize carbon dots and activated carbon from rice wastes in two-in-one approach

1.2.2 To improve the specific capacitance and energy density by using the carbon dots as an additive

1.2.3 To prepare an alternative polymer electrolyte from rice and carbon dots

1.2.4 To fabricate the supercapacitor from the prepared electrode and electrolyte

1.3 Scope and limitation of the study

This research divides into 2 subjects based on raw materials for synthesis of activated carbon and carbon dots including

1.3.1 Synthesis of activated carbon and carbon dots from rice straw

1.3.1.1 To synthesize the carbon dots and activated carbon from rice straw as a raw material using the hydrothermal method and thermal activation, respectively.

1.3.1.2 To study the effects of the following activation parameters on the properties of activated carbon

1.3.1.2.1 Ratio of the chemical activating agent to carbon char

1.3.1.2.2 Activation temperature

1.3.1.2.3 Activation time

1.3.1.3 Characterization of prepared carbon dots

1.3.1.3.1 Structure characterizations

- Fourier transform infrared spectroscopy (FT-IR)

- X-ray photoelectron spectroscopy (XPS)

1.3.1.3.2 Size measurements

- Transmission electron microscope (TEM)

1.3.1.3.3 Optical properties

- UV-visible spectroscopy

- Fluorescence spectroscopy

1.3.1.4 Characterization of prepared activated carbon

1.3.1.4.1 Morphological characterizations

- Nitrogen adsorption-desorption

- Scanning electron microscope (SEM)

1.3.1.4.2 Electrochemical properties

- Cyclic voltammetry (CV)

1.3.1.5 Preparation of rice electrolyte via following parameters

CHAPTER 2
REVIEW OF LITERATURE

2.1 Supercapacitor

Supercapacitor is a highly effective energy storage device consisting of three main components: electrode, electrolyte, and separator as shown in Figure 2.1. The supercapacitor has received wide attention based on several advantages, including fast charge-discharge rate, high power density, long-term cyclability, and excellent stability (Ashritha & Hareesh, 2020; S. Liu, Wei, & Wang, 2020; Saikia et al., 2020; Vinodh et al., 2020).
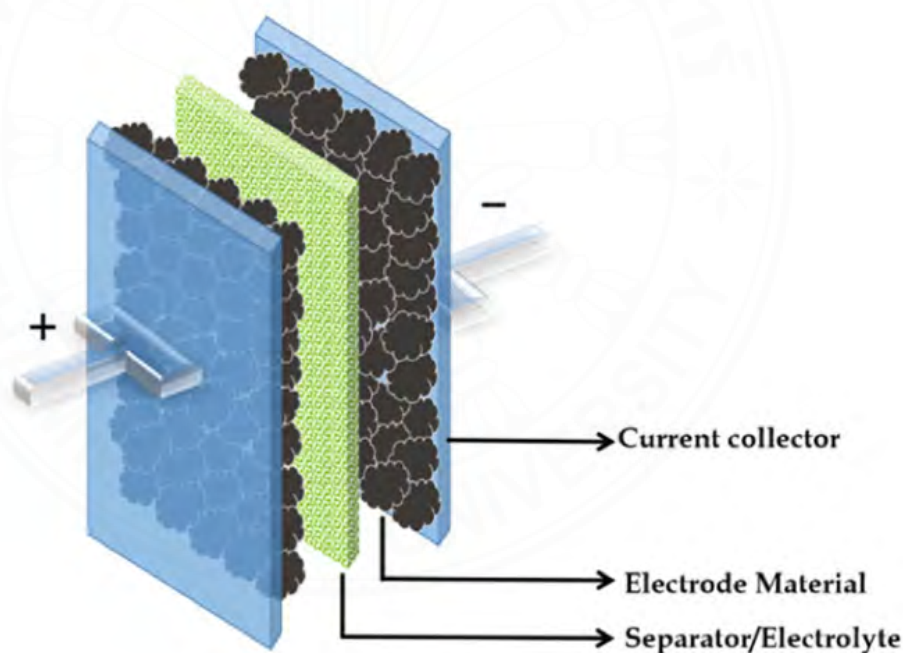
Figure 2.1 Components of supercapacitor. Adapted from Samantara, Aneeya, K., Ratha, & Satyajit, 2018, New York City: Springer.

Based on electrode materials, the supercapacitor can be divided into three types: electric double-layer capacitors (EDLC), pseudocapacitors (PC), and hybrid

capacitors (HSC). These three types are mainly different in the electrode materials and charge storage mechanisms as summarized in Table 2.1.

Table 2.1

Classification of supercapacitors based on the electrode materials and the charge storage mechanisms. (S. Liu et al., 2020; Vinodh et al., 2020; Zhong et al., 2015)

Types List	Electric double-layer capacitors (EDLC)	Pseudocapacitors (PC)	Hybrid capacitors (HSC)
Electrode material	Carbon (e.g., activated carbon, graphene, carbon nanotubes)	Noble metal (e.g., Pt, Au) Metal oxide (e.g., RuO_2, MnO_2), Conducting polymer (e.g., polyaniline)	Asymmetric (e.g., anode: PC-type materials, cathode: EDLC-type materials), Symmetric composite
Charge mechanism	Electrostatically	Electrochemically	Electrostatically and electrochemically

The supercapacitor and battery are competitive in several aspects with distinct advantages and disadvantages as summarized in Table 2.2.

Table 2.2

Comparison between supercapacitor and battery. (Ashritha & Hareesh, 2020)

Parameter	Supercapacitor	Battery
Charge time	0.3-30 seconds	1-5 hours
Discharge time	0.3-30 seconds	0.3-3 hours
Cycle life	>10,000	500-2,000
Energy density (Wh kg^{-1})	1-10	1-100
Power density (W kg^{-1})	~1,000	5-200
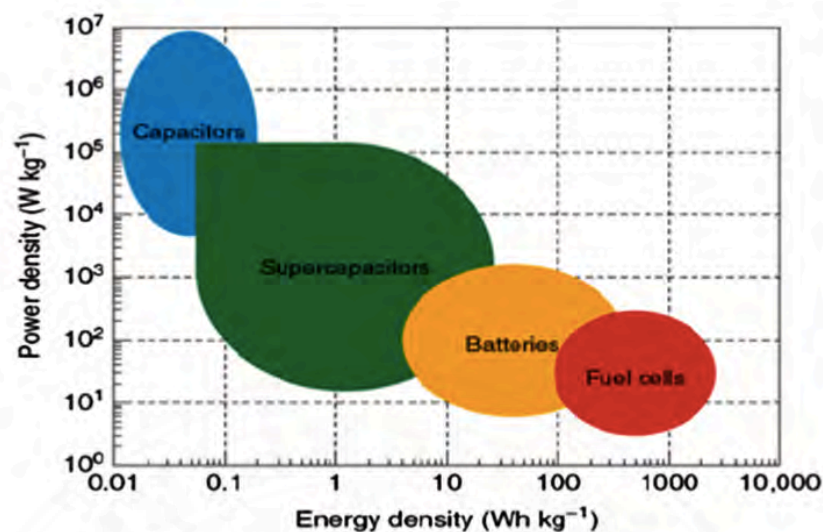
Figure 2.2 Ragone plot comparing various energy storage and conversion devices. Adapted from "Influence of various Activated Carbon based Electrode Materials in the Performance of Super Capacitor," by K. M. Ajay and M. N. Dinesh, 2018, *IOP Conference Series: Materials Science and Engineering, 310*, p. 12083. Copyright 2018 by IOP Publishing.

Despite several advantages of the supercapacitor, the energy density of the supercapacitor is lower than that of the lithium-ion battery. As shown in Figure 2.2, it can be observed that both power density and energy density of the supercapacitor lies in between conventional capacitors and batteries. Therefore, both capacitance and potential window need to be improved to enhance the energy density.

2.1.1 Electrode material

The electrode materials contribute to the supercapacitor performances. Carbon-based materials, such as activated carbon, graphene, and carbon nanotubes, have been used for electric double-layer capacitors (EDLC). Metal oxides, metal sulfides, and conducting polymers are electrode materials for pseudocapacitors. Composite materials or asymmetric pseudo/EDLCs are electrode materials for hybrid capacitors.

2.1.2 Electrolyte

To enhance the energy density of supercapacitors, the suitable electrolytes need to be developed. A wide potential window of an electrolyte will be

advantageous for increasing the energy density of the supercapacitor. A variety of electrolytes have been developed and used in supercapacitors with variable potential windows. For example, aqueous electrolytes provide a potential window from 1.0 V to 1.3 V, while organic and ionic liquid electrolytes can generate the wider window of about 2.5–2.7 V, and above 3.5 V, respectively. Various types of electrolytes have been used in supercapacitors as shown in Figure 2.3.
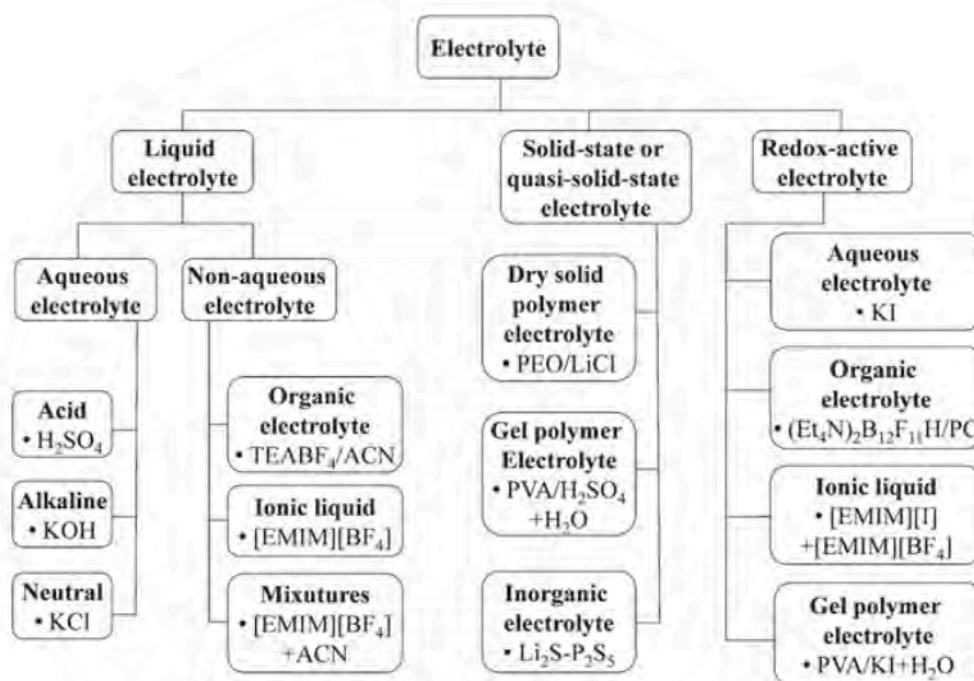
Figure 2.3 Various types of electrolytes that have been implemented in supercapacitor. Adapted from "A review of electrolyte materials and compositions for electrochemical supercapacitors," by C. Zhong et al, 2015, *Chemical Society Reviews, 44*, p. 7490. Copyright 2015 by The Royal Society of Chemistry.

2.2 Activated carbon

Activated carbon (AC) is a carbon-based material which has attracted attention due to its large specific surface area, narrow pore size distribution, high conductivity, low-toxicity, and good thermochemical stability (Heidarinejad et al.,

2020; Rashidi & Yusup, 2020). Activated carbon has been used in a wide range of applications including adsorption (Dao & Le Luu, 2020; D. Zhou et al., 2020), waste-water treatment (Santos, de Jesus, da Silva, & Pontes, 2020), drug delivery (Miriyala, Ouyang, Perrie, Lowry, & Kirby, 2017), and energy storage (Eleri et al., 2020; Lu, Cao, Hao, Zhou, & Wang, 2020; Rajasekaran & Raghavan, 2020; Ukkakimapan et al., 2020; Usha Rani, Nanaji, Rao, & Deshpande, 2020; Yakaboylu et al., 2021). As shown in Figure 2.4 the three pore groups of activated carbon consisted of macropore, mesopore, and micropore.
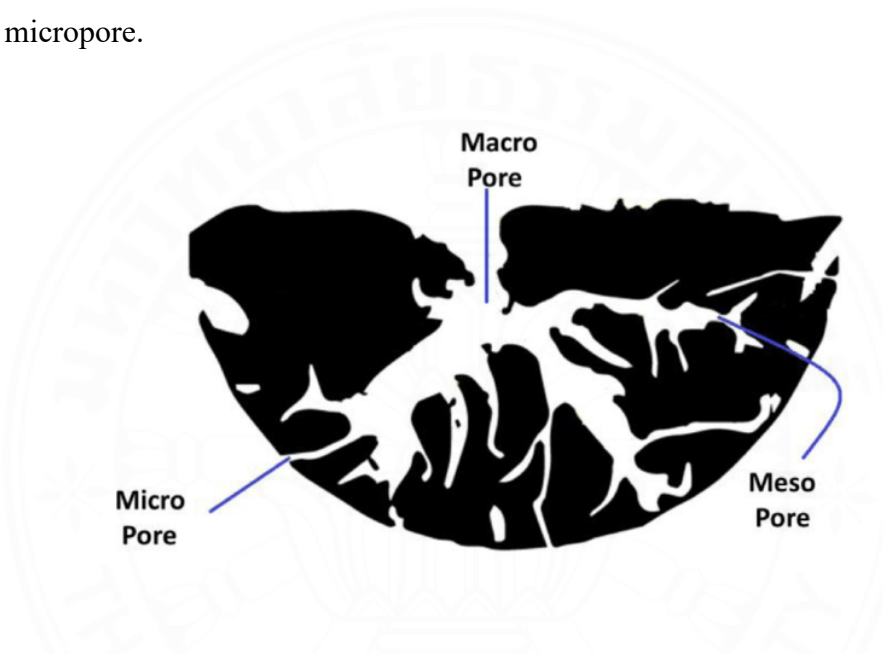
Figure 2.4 Different types of pores in activated carbon. Adapted from "Carbon Nanomaterials for the Treatment of Heavy Metal-Contaminated Water and Environmental Remediation," by R. Baby, S. Bullo, and M. Hussein, 2019, *Nanoscale Research Letters, 14*, p. 11. Copyright 2019 by Rabia Baby, Bullo Saifullah, and Mohd Zobir Hussein.

The activated carbon can be prepared in two approaches namely: physical and chemical activations (Heidarinejad et al., 2020). The physical activation is a two-step process that involves the carbonization in the atmosphere and activation in atmospheric oxidizing gases such as steam and carbon dioxide at high temperature (800-1100°C), whereas the chemical activation is usually used in biomass resources. The biomass can be directly activated or pre-treated to bio-char. In the first stage, the precursors are saturated with oxidizing and dehydrating chemicals, called impregnation. After

impregnation, the suspension was dried, and the remaining mixture was subsequently activated in the presence of chemicals at high temperature (400-900ºC) under an inert gas atmosphere. The activating agents can deeply penetrate into the carbon structure, leading to the development of small pores in the activated carbon and increased surface area. Figure 2.5 shows an example of activated carbon production from biomass and char via physical or chemical activations.
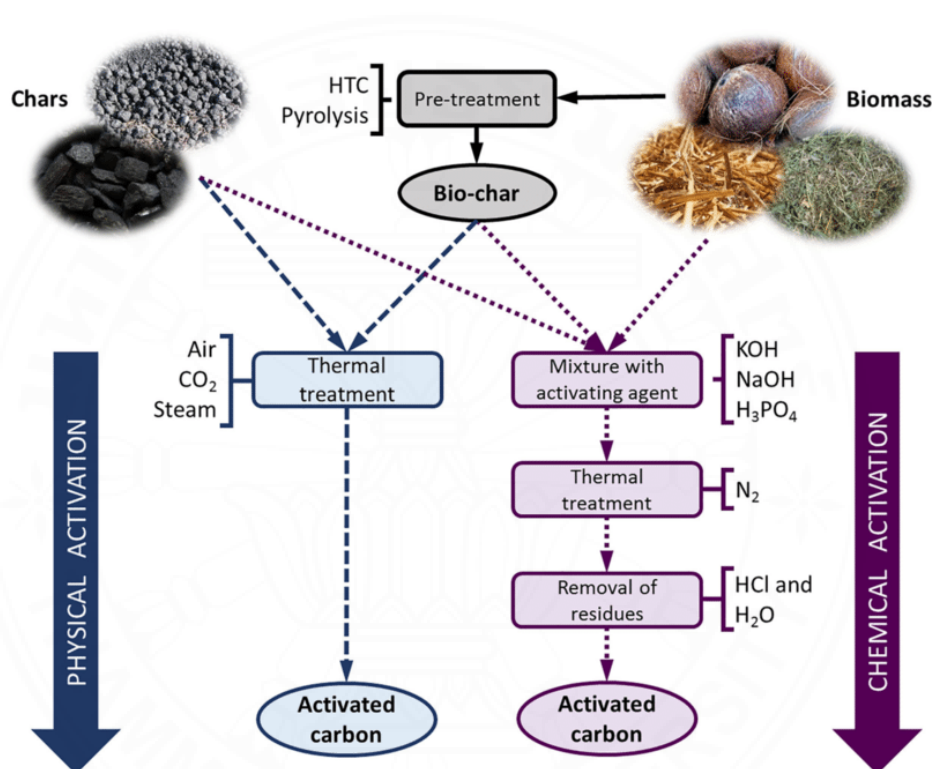
Figure 2.5 The schematic production process of activated carbons, from biomass and char, by physical or chemical activation. Adapted from "Energy Storage in Supercapacitors: Focus on Tannin-Derived Carbon Electrodes," by J. Castro-Gutiérrez, A. Celzard, and V. Fierro, 2020, *Frontiers in Materials, 7*, p.217. Copyright 2020 by Castro-Gutiérrez, Celzard and Fierro.

The advantages and disadvantages of physical activation and chemical activation were summarized in Table 2.3.

Table 2.3

The advantages and disadvantages of physical activation and chemical activation.

Types / List	Physical activation	Chemical activation
Advantages	Inexpensive method, chemical-free	Lower activation temperature, shorter processing time, higher carbon efficiency
Disadvantages	Long activation time, low adsorption capacity, high energy consumption	Toxic wastewater from washing step

Although physical and chemical activation methods present different advantages and disadvantages, chemical activation is more popular for the activated carbon preparation because it is convenient and effectively creates porous structure. A number of precursors for the preparation of activated carbon by chemical activation are summarized in Table 2.4.

Table 2.4

Activated carbon from various precursors prepared by chemical activation.

Precursors	Chemical activator and conditions	Specific surface area $(m^2\ g^{-1})$	Specific capacitance $(F\ g^{-1})$	Energy density $(Wh\ kg^{-1})$	References
Sawdust	KOH 600 °C, 1 h	3083	160 (0.25 A g^{-1})	49	(Eleri et al., 2020)
Miscanthus grass	KOH 800 °C, 1 h	1816	162 (0.5 A g^{-1})	8	(Yakaboylu et al., 2021)
Eucalyptus globulus seed	KOH 900 °C, 1 h	2389	150 (1 A g^{-1})	-	(Rajasekaran & Raghavan, 2020)
Durian husk	NaOH 900 °C, 1 h	2578	145 (0.1 A g^{-1})	32	(Ukkakimapan et al., 2020)
Pitaya peel	KOH 800 °C, 2 h	1872	255 (1 A g^{-1})	-	(Lu et al., 2020)
Corn husk	KOH 800 °C, 2 h	1370	127 (1 A g^{-1})	4.4	(Usha Rani et al., 2020)
Laminaria japonica	KOH 700 °C, 2 h	1902	192 (0.1 A g^{-1})	-	(Cheng et al., 2020)
Coconut coir pith	NaOH 700 °C, 1 h	2056	232 (0.1 A g^{-1})	-	(Sesuk et al., 2019)

As shown in Table 2.4, the chemicals widely used as potential activators are alkaline groups. Potassium hydroxide (KOH) has been extensively used due to its ability to produce activated carbon with a high surface area and narrow pore size distribution.

The pore formation and structural deformation were studied during chemical activation processes using KOH as a chemical activator and carbon sphere

(CS) as a considered carbon. The first step is the dissociation of KOH in water according to Equation 2.1.

$$KOH_{(s)} \rightarrow K^+_{(aq)} + OH^-_{(aq)} \qquad \text{(Equation 2.1)}$$
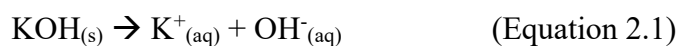
In aqueous solutions, the potassium ions (K^+) are randomly distributed and freely move. During the activation process, these ions can induce the formation of pores in the carbon structure via the penetration of the energized potassium ions into the carbon sphere. After the activation process, the activated carbon was then washed for several times to remove the excess potassium ions. Different KOH concentration could provide different formation and structure of the created pores on the activated carbon surface as shown in Figures 2.6 and 2.7.
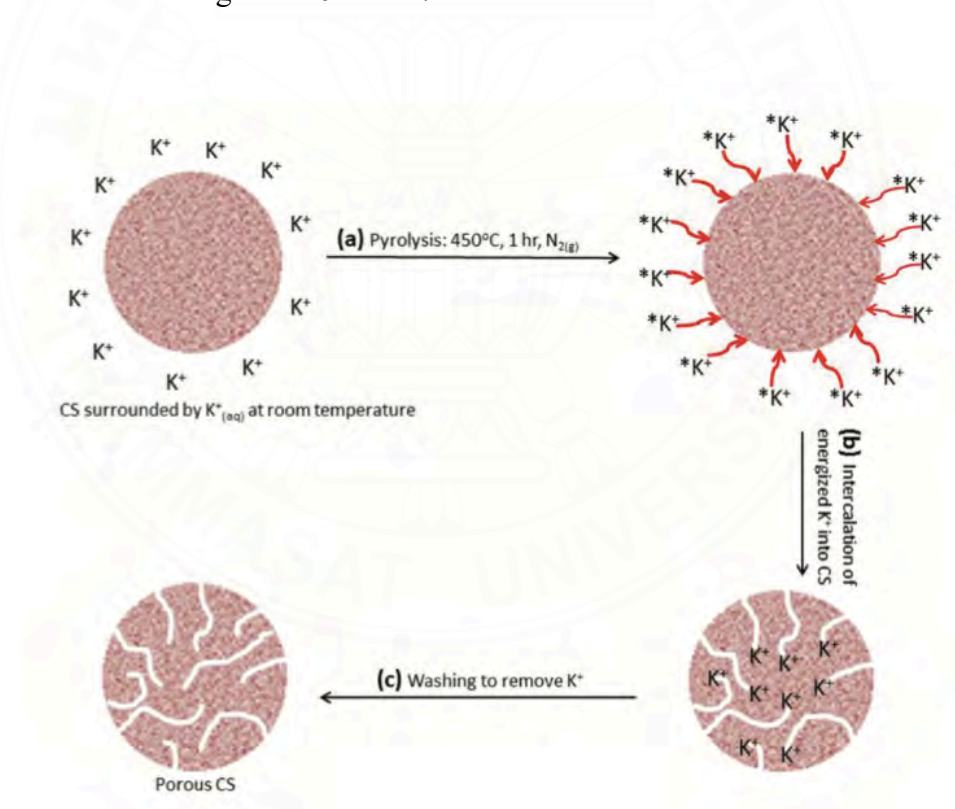
Figure 2.6 Pore formation processes at lower KOH concentrations. Adapted from "Understanding Pore Formation and Structural Deformation in Carbon Spheres During KOH Activation," by M. S. Musa, M. M. Sanagi, H. Nur, and W. A. Wan Ibrahim, 2015, *Sains Malaysiana, 44*, p. 616. Copyright 2015 by Sains Malaysiana.
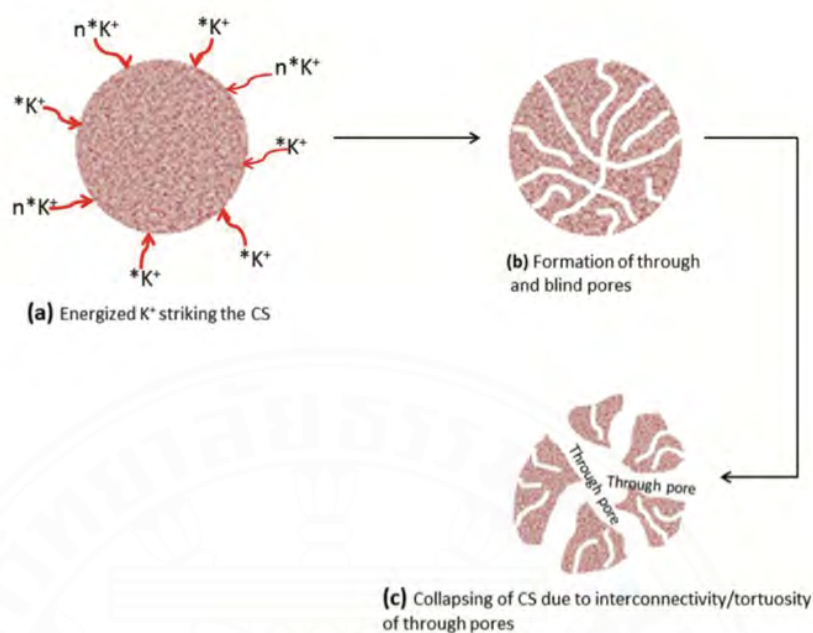
Figure 2.7 Pore formation and structural collapse of carbon spheres at higher KOH concentrations. Adapted from "Understanding Pore Formation and Structural Deformation in Carbon Spheres During KOH Activation," by M. S. Musa et al, 2015, *Sains Malaysiana, 44*, p. 617. Copyright 2015 by Sains Malaysiana.

2.3 Raw materials: rice, rice straw, and rice husk

Figure 2.8 The images of rice (left), rice straw (middle), and rice husk (right)

Rice (Oryza sativa) is one of the popular food plants in Thailand. Rice production has been in high demand every year, especially in Asia and Africa.

Moreover, rice has abundant nutrients such as carbohydrates, proteins, fiber, fat, and sugar. Its straw and husk are also the largest agricultural byproduct from harvesting (Figure 2.8). As shown in Figure 2.9, the production of rice reached a historically high level of 7.4 million tonnes during in 2017-2018. Meanwhile, the numbers of rice straw and rice husk are increasing from byproduct of rice harvesting.
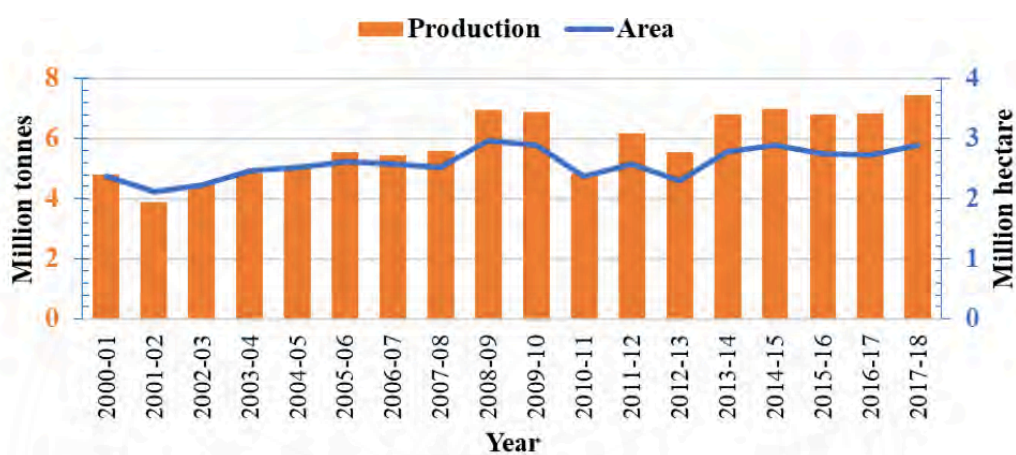
Figure 2.9 Annual rice production and area under cultivation. Adapted from "A comparative assessment of rice straw management alternatives in Pakistan in a life cycle perspective," by A. Mahmood and S.Gheewala, 2020, *Journal of Sustainable Energy & Environment, 11*, p. 21. Copyright 2020 By Journal of Sustainable Energy and Environment.

Rice straw and rice husk, considered as lignocellulosic biomass, comprise three main components: lignin, cellulose, and hemicelluloses as shown in Figure 2.10. The lignocellulosic components of rice straw and rice husk as shown in Table 2.5. The rice straw and rice husk are thus a promising biomass candidate for the preparation of the activated carbon as an electrode material for supercapacitor applications.
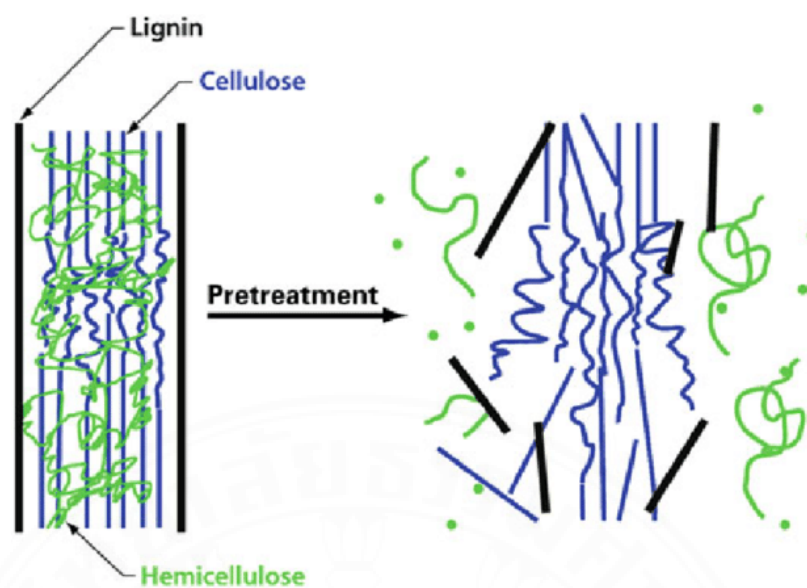
Figure 2.10 Major components of lignocellulosic biomass. Adapted from "Fuels and Chemicals from Hemicellulose Sugars," by Z. Ji et al, 2012, *Advances in Biochemical Engineering/biotechnology, 128*, p. 203. Copyright 2012 by Springer-Verlag Berlin Heidelberg.

Table 2.5

Lignocellulosic components of rice straw and rice husk. (Janewit, Worasuwannarak, & Pipatmanomai, 2008)

Biomass	Cellulose	Hemicellulose	Lignin	Extractive matter
Rice straw	32.0	35.7	22.3	10.0
Rice husk	28.6	28.6	24.4	18.4

Because of their high carbon content, the rice straw and rice husk have been reported to be used as a precursor for preparing the activated carbon applied for the electrode materials in the supercapacitor. The activated carbon electrodes from rice wastes in different electrolytes provide a variety of potential window, specific capacitance, and energy density as summarized in Table 2.6.

Table 2.6

Electrochemical performance of rice waste-derived activated carbon electrode in aqueous and organic electrolyte.

Electrode material	Electrolyte	Potential window (V)	Specific capacitance (F g^{-1})	Energy density (Wh kg^{-1})	References
Rice straw (AC)	1 M H$_2$SO$_4$	0.8	357 (0.5 A g^{-1})	29.3	(Chen et al., 2018)
Rice straw (AC)	([EMIM][BF$_4$])	2.5	80 (0.1 A g^{-1})	17.4	(Sudhan, Subramani, Karnan, Ilayaraja, & Sathish, 2017)
Rice straw (AC)	6 M KOH	1.0	400 (0.1 A g^{-1})	13.9	(H. Jin et al., 2018)
Rice straw (AC)	6 M KOH	1.0	420 (1 A g^{-1})	11.1	(G. Zhou et al., 2020)
Rice straw (AC)	0.5 M H$_2$SO$_4$	1.0	93 (10 mV s^{-1})	-	(Nam, Choi, Genuino, & Capareda, 2018)
Rice husk (AC)	0.5 M K$_2$SO$_4$	1.0	205 (2 mV s^{-1})	-	(Le Van & Luong Thi Thu, 2019)
Rice husk (AC)	6 M KOH	1.0	315 (0.5 A g^{-1})	10.9	(D. Liu, Zhang, & Huang, 2019)
Rice husk (AC)	6 M KOH	1.0	147 (0.1 A g^{-1})	5.1	(Teo et al., 2016)
Rice husk (AC)	0.5 M K$_2$SO$_4$	1.0	172.3 (5 mV s^{-1})	-	(Le Van & Luong Thi, 2014)
Rice husk (AC)	6 M KOH	0.8	250 (1 A g^{-1})	22.2	(Xu et al., 2014)

2.4 Polysaccharide based polymer electrolyte

Polysaccharides are complex biomacromolecules consisting of monosaccharides connected via glycosidic bond. The glycosidic bonds consist of an oxygen atom bridging with two carbon rings. The bond is formed from the condensation between two hydroxyl groups. Because one molecule of water is expelled, the reaction is called a dehydration reaction. Examples of a polysaccharide include cellulose, chitin, starch, and glycogen as shown in Figure 2.11. Polysaccharides have become popular biopolymers because of their high abundance, wide distribution, and low cost of production.

Cellulose

Chitin

Amylose

Amylopectin
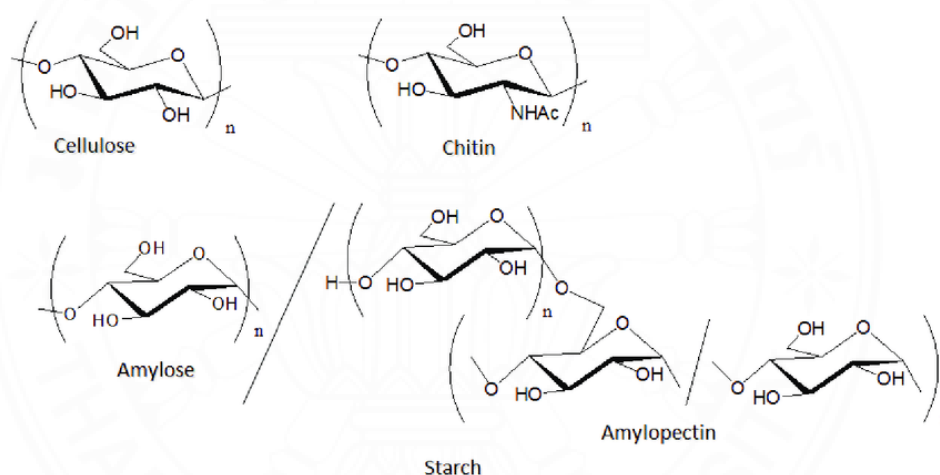
Starch

Figure 2.11 Structures of cellulose, chitin, and starch. Adapted from "Fabrication and Characterization of Polysaccharide Ion Gels with Ionic Liquids and Their Further Conversion into Value-Added Sustainable Materials," by A. Takada and J. Kadokawa, 2015, *Biomolecules, 5*, p. 245. Copyright 2015 by Akihiko Takada and Jun-ichi Kadokawa.

Polysaccharides based polymer as an electrolyte using in supercapacitor were summarized in Table 2.7.

Table 2.7

Electrochemical performance of the carbon-based electrode in starch-based electrolytes.

Electrode	Electrolyte	Potential window (V)	Specific capacitance (F g^{-1})	Energy density (Wh kg^{-1})	References
AC	Manihot esculenta starch powder	0.8	240 (0.5 mA)	17	(Kasturi, Ramasamy, Meyrick, Sung Lee, & Kalai Selvan, 2019)
AC	Powdered neem gum in LiBF$_4$	1.0	640 (0.5 A g^{-1})	22.2	(Dhar et al., 2020)
GO	Corn starch	1.0	18.4 (10 mV s^{-1})	-	(Ahuja et al., 2020)
AC	CMC blended with kappa carrageenan and doped with NH$_4$NO$_3$	1.0	25.83 (2 mV s^{-1})	-	(Zainuddin, Rasali, Mazuki, Saadiah, & Samsudin, 2020)
AC	CS:MC: NH$_4$SCN	0.9	76.7 (10 mV s^{-1})	8.63	(Aziz, Hamsan, Abdullah, & Kadir, 2019)
AC	AmNTFSI-based iota-carrageenan	1.0	12.7 (0.4 A g^{-1})	-	(Farhana et al., 2019)

2.5 Carbon dots

Carbon dots (CDs) are zero-dimensional carbon-based nanomaterials with the size of around 2 to 10 nm (Y. Wang, Sun, He, & Feng, 2020). Since their discovery in 2004, the carbon dots have been studied and applied in a variety of applications including bio-imaging (Atchudan et al., 2021; L. Wang & Zhou, 2014), drug delivery (Nair, Haponiuk, Thomas, & Gopi, 2020), biomedicine (Jaleel & Pramod, 2018), sensors (Kumari & Chaudhary, 2020; Wen et al., 2020), catalytic (Prasannan & Imae, 2013; Y. Wang et al., 2020), printing and fluorescent ink (Y. Wang et al., 2020), and energy storage (Kumar et al., 2016; Moreno Araújo Pinheiro Lima & de Oliveira, 2020) (Figure 2.12). The carbon dots have attracted attention because of their promising properties such as extremely size in nanometer, diverse functional groups (e.g., hydroxyl, carbonyl) on the surface, high water-solubility, and photoluminescence properties. Moreover, carbon dots are also environmentally friendly and have low cytotoxicity due to the absence of heavy metal component like quantum dots (Long et al., 2021; Rani, Ng, Ng, & Mahmoudi, 2020; Y. Wang et al., 2020).
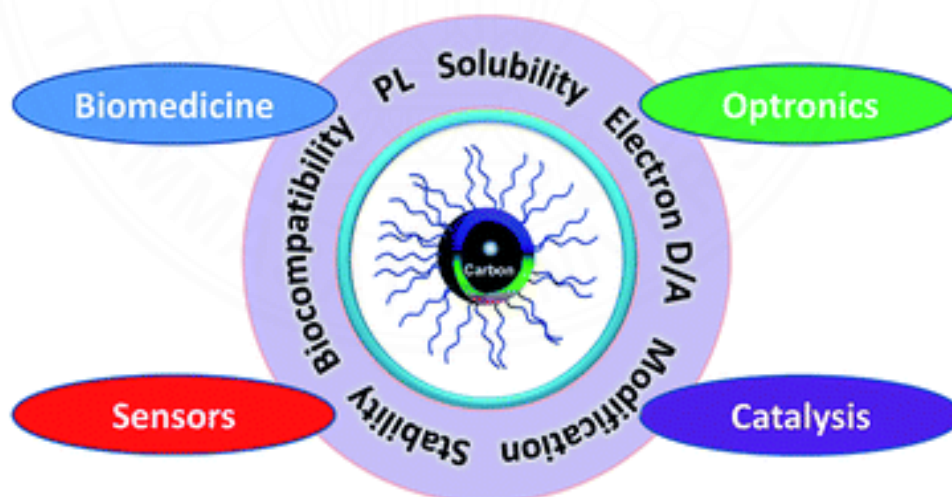
Figure 2.12 Properties and applications of carbon dots. Adapted from "Carbon quantum dots: synthesis, properties and applications," by Y. Wang and A. Hu, 2014, *Journal of Materials Chemistry C, 2*, p. 6922. Copyright 2014 by The Royal Society of Chemistry.

Various synthetic methods have been used to prepare the carbon dots. The synthesis methods can be classified into top-down and bottom-up approaches as shown in Figure 2.13. The features of the different synthetic methods used for the preparation of carbon dots are summarized in Table 2.8.
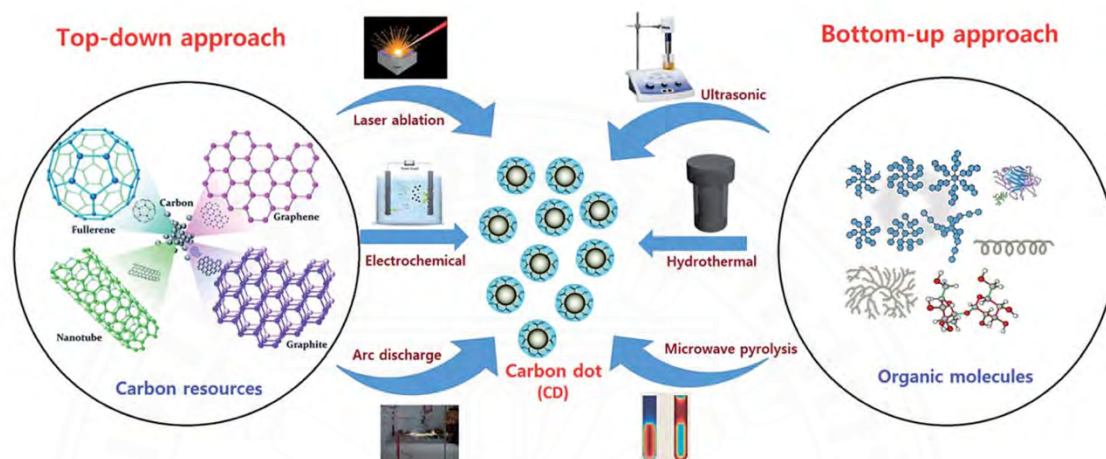
Figure 2.13 The various synthetic method of carbon dots. Adapted from "Carbon Nanodots: A Review—From the Current Understanding of the Fundamental Photophysics to the Full Control of the Optical Response," by A. Sciortino, A. Cannizzo, and F. Messina, 2018, *Journal of Carbon Research, 4*, p. 70. Copyright 2018 by Alice Sciortino, Andrea Cannizzo, and Fabrizio Messina.

Table 2.8

The features of the different synthetic methods used for the preparation of CDs.

Synthetic methods	Advantages	Disadvantages
Chemical ablation	Most accessible and various sources	Hard conditions, strong processes, multiple steps, poor control over sizes
Electrochemical carbonization	Controllable size and nanostructure, stable, one-step	Few small molecule precursors
Laser ablation	Rapid, effective, surface states tunable	Low quantum yield, poor control over sizes, modification is needed
Microware irradiation	Rapid, scalable, cost effective, environmentally friendly	Poor control over sizes
Hydrothermal/ solvothermal treatment	Cost effective, environmentally friendly, non-toxic	Poor control over sizes

The precursors for synthesizing the carbon dots can be divided into chemical precursors, natural precursors, and wastes which are abundant carbon sources. Examples of carbon dots precursors, synthesis methods, and applications are shown in Table 2.9.

Table 2.9

Examples of carbon dots precursor, synthesis method, and applications.

Precursors	Synthetic methods	Applications	References
Hyaluronic acid	Hydrothermal	Sensor	(Wen et al., 2020)
Polyethylene glycol-400	Sonication	Energy storage	(Kumar et al., 2016)
1,6-hexanediamine dihydrochloride	Microwave	Sensor and cell imaging	(Ding, Deng, Chen, & Jin, 2020)
Milk	Hydrothermal	Bio-imaging	(L. Wang & Zhou, 2014)
Green tea leaf residue	Pyrolysis	Sensor	(Hu, Jiao, & Xu, 2020)
Orange peels	Hydrothermal	Photocatalytic	(Prasannan & Imae, 2013)
Banana peels	Hydrothermal	Bio-imaging	(Atchudan et al., 2021)
Plastic wastes	Hydrothermal	Biosensor	(Kumari & Chaudhary, 2020)

CHAPTER 3
RESEARCH METHODOLOGY

3.1 Materials and chemicals

Rice straw and rice husk were obtained from a local rice paddy field in Pathumthani, Thailand and rice was obtained from a local supermarket. All chemicals were purchased from Sigma-Aldrich and were of analytical grade. Cellulose dialysis membrane (MWCO = 1 kDa) was purchased from Spectrum Labs. Nickel foam sheets (1 μm thick) were purchased from a local supplier in Thailand. Deionized water was used in all experiments.

3.2 Methods and preparations

3.2.1 Synthesis of activated carbon (AC) and carbon dots (CDs)
3.2.1.1 Synthesis of AC and CDs from rice straw

Rice straw was washed with plenty of water, sun-dried for 36 h, cut, and crushed into small pieces. The crushed, dried rice straw (5 g) was mixed with 1.5 M phosphoric acid solution (100 mL) and ultrasonicated for 15 min. The mixture was transferred to a Teflon-lined autoclave and heated at 220 °C for 5 h. After the reaction was completed, the reaction mixture was cooled down to room temperature, ultrasonicated for 15 min, and filtered to separate carbon char and filtrate. The filtrate was kept for the extraction of CDs. The carbon char was washed, dried and crushed to a fine powder form. The carbon char (3 g) was mixed with KOH as a chemical activating agent in the presence of deionized water (60 mL) and then heated to 90 °C for 1 h to form a slurry. The slurry was pyrolyzed with a constant flow of N_2 gas. The resultant material was washed with hot deionized water and 1 M HCl and dried for 24 h in an oven at 80 °C to obtain rice straw activated carbon (RSAC). The KOH/carbon char weight ratio, activation temperature, and activation time varied as summarized in Table 3.1.

Table 3.1

Experimental details for the preparation of activated carbon from rice straw carbon char (RSAC).

Sample ID	KOH/carbon char weight ratio (w/w)	Activation temperature (°C)	Activation time (h)
RSAC1	0.5:1	800	1
RSAC2	1:1	800	1
RSAC3	1:0.5	800	1
RSAC4	1:1	700	1
RSAC5	1:1	900	1
RSAC6	1:1	800	1.5
RSAC7	1:1	800	2

The filtrate was neutralized with 10 M NaOH solution. The solution was purified using a dialysis membrane (MWCO = 1 kDa) for 36 h in deionized water, deionized water was replaced every 6 h and then freeze-dried to yield the CDs as brown solid powder (1.13 g, 22.7 %).

3.2.1.2 Synthesis of AC and CDs from rice husk

10 g of crushed rice husk was mixed with 50 mL of 2.5 M HNO_3 in a beaker and ultrasonicated 15 min. Then, the mixture was transferred to a Teflon autoclave and heated to 200 °C for 6 h. After the reaction was completed, it was ultrasonicated for 15 min and filtered to obtain the rice husk carbon char and dark brown solution. The dark brown solution was neutralized with 10 M NaOH and purified by using a dialysis membrane for 48 h. After that, the solution was freeze-dried to obtain the CDs powder.

The rice husk carbon char was impregnated with KOH as an activating agent in ratio 1:1 (%w/w) and then activated at 800 °C for 1 h in a tube furnace under N_2 atmosphere. After the activation was completed, the activated carbon was rinsed with hot deionized water until a neutral pH in order to remove KOH residues and then dried again to obtain the rice husk activated carbon (RHAC).

3.2.2 Fabrication of working electrode

3.2.2.1 Fabrication of working electrode using RSAC

Rice straw activated carbon and poly(vinylidene fluoride) (PVDF) as a binder were mixed in *N*-methylpyrrolidone (NMP) in a weight ratio of 95:5 %w/w to form a slurry. The slurry was coated on a piece of nickel foam sheet and dried at 80 °C for 1 h prior to characterization. The electrode was then immersed into an electrolyte for 24 h prior to electrical characterization.

3.2.2.2 Fabrication of working electrode using RHAC

The rice husk activated carbon was mixed with PVDF as a binder and carbon black as a conductive agent in a ratio of 90:5:5 (%w/w) in N-methyl-2-pyrrolidone (NMP) as a solvent. The mixture was coated on a nickel foam sheet as a current collector and then dried to obtain the RHAC electrode (approximately mass loading of 5 mg). For the fabrication of RHAC/CDs electrode, the CDs were added to the mixture in a ratio of RHAC, CDs, PVDF, and carbon black of 85:5:5:5 (%w/w) in the NMP solvent.

3.2.3 Preparation of electrolytes

3.2.3.1 Polyvinyl alcohol electrolyte

As a standard electrolyte, H_3PO_4/poly(vinyl alcohol) (PVA) electrolyte was prepared. PVA (10 g) was added to deionized water (100 mL) in a beaker and was continuously stirred for 1 h until a clear solution of PVA was obtained. Then 10 g of H_3PO_4 was added to the PVA solution with continuous stirring for 30 min to obtain a H_3PO_4/PVA electrolyte.

3.2.3.2 Rice electrolyte

Rice grains (10 g) were added to deionized water (100 mL) in a beaker and the mixture was heated at 100 °C under continuous stirring for 30 min until it became a viscous mixture and then a concentrated phosphoric acid (5, 10, 15, 20, and 25 g) was added with continuous stirring for 30 min to obtain homogeneous H_3PO_4/rice electrolyte. For the carbon dot-added electrolytes, CDs (20, 60, and 100

mg) were added to the homogenous H_3PO_4/rice mixture, which was then stirred for an additional 30 min.

3.3 Characterizations

3.3.1 Characterization of carbon dots

The UV-visible absorption and fluorescence emission spectra of CDs were measured using a UV-visible spectrometer (Shimadzu, UV-1700 PharmaSpec) and fluorescence emission spectrometer (Jasco, FP-6200), respectively. The Fourier Transform Infrared (FT-IR) spectra of CDs was measured using an FT-IR spectrometer (Perkin Elmer, Spectrum 2000) and using KBr powder pressed pellets. An X-ray photoelectron spectrometer (AXIS ULTRADLD, Kratos Analytical) was used to characterize the surface element and compositions of CDs. A transmission electron microscopy (TEM) image of CDs was investigated using an FEI Tecnai G2 F20 microscope. The zeta potential of carbon dot solution was measured using a Nano Particle Analyzer (HORIBA, Nano Partica SZ-100) at 25°C with a scattering angle of 173°.

3.3.2 Characterization of an activated carbon

The surface morphology of activated carbon was analyzed using a scanning electron microscope (Hitachi, S-3400). The samples were mounted on a carbon tape. Specific surface area, pore size, and pore volume were measured using nitrogen adsorption-desorption (Quantachrome, Autosorb iQ-C). The Brunauer-Emmett- Teller (BET) method was adopted to calculate the specific surface area and the Barret-Joner-Halenda (BJH) method was used to calculate the pore volume and pore size distribution.

3.4 Electrochemical measurements

The electrochemical characterizations were performed using a potentiostat/galvanostat (μAutolab, PGSTAT204). Two types of electrochemical cells were used: (a) a three-electrode cell containing 1) RSAC/PVDF and 2)

RHAC/CDs/PVDF/CB as a working electrode, platinum wire as a counter electrode, and an Ag/AgCl reference electrode and (b) a two-electrode cell was used for Swagelok cell. The three-electrode cell was characterized using cyclic voltammetry (CV) and electrochemical impedance spectroscopy (EIS). The EIS was conducted in the frequency range between 100 kHz and 100 mHz with an amplitude of 10 mV. The two-electrode cell was characterized using galvanostatic charge-discharge (GCD) measurement. The CV in PVA electrolyte was carried out at the potential range of -0.4 to 1.2 V at various scan rates from 10 to 100 mV s^{-1}. The CV and GCD experiments using rice electrolyte were carried out at the potential range of -0.7 to 1.7 V at various scan rates from 10 to 100 mV s^{-1} and current densities ranging from 0.8 to 5 A g^{-1}, respectively. The CV and GCD measurements using 6 M KOH were performed at the potential range of 0.0 to -1.0 V at various scan rates from 10 to 100 mV s^{-1} and current densities ranging from 0.5 to 4 A g^{-1}, respectively. A Swagelok cell was utilized to measure the cyclability using Whatman filter paper and nickel foam with a diameter of 1 cm as separator and current collector, respectively. The specific capacitance (C_{sp}) values of the electrode were calculated from cyclic voltammogram using the following equations:

$$C_{sp} = \frac{I}{mS} \qquad \text{(Equation 3.1)}$$

$$C_{sp} = \frac{I\Delta t}{m\Delta V} \qquad \text{(Equation 3.2)}$$

where C_{sp} (F g^{-1}) is the specific capacitance, I (A) is the average current, m (g) is the mass of the material, S (V s^{-1}) is the scan rate of the applied ramp voltage, Δt (s) is the time interval of the voltage change for the supercapacitor cells, and ΔV (V) is the working potential window. The energy density and the power density were calculated using the following equations:

$$E = \frac{C(\Delta V)^2}{2} \qquad \text{(Equation 3.3)}$$

$$P = \frac{E}{t} \qquad \text{(Equation 3.4)}$$

where E (Wh kg^{-1}) is energy density of the supercapacitor system, C (F g^{-1}) is the total specific capacitance, P (W kg^{-1}) is power density, and t is the discharge time (h).

CHAPTER 4
RESULTS AND DISCUSSION

4.1 Synthesis, characterization, and application of activated carbon and carbon dots from rice straw

4.1.1 Synthesis and characterization of RSAC

Rice straw is a common agricultural waste which is rich in carbon due to the presence of cellulose, hemicellulose, and lignin. In this work, a two-in-one approach was used for preparing both activated carbon and CDs from rice straw. After hydrothermal treatment of the rice straw, the carbon char and CDs were separated by simple gravitational filtration. The carbon char was proceeded for the preparation of activated carbon and then the electrode whereas the CDs were used as additives in electrolyte, which will be discussed later. In this work, RSAC and RSCDs refer to rice straw activated carbon and rice straw carbon dots, respectively.
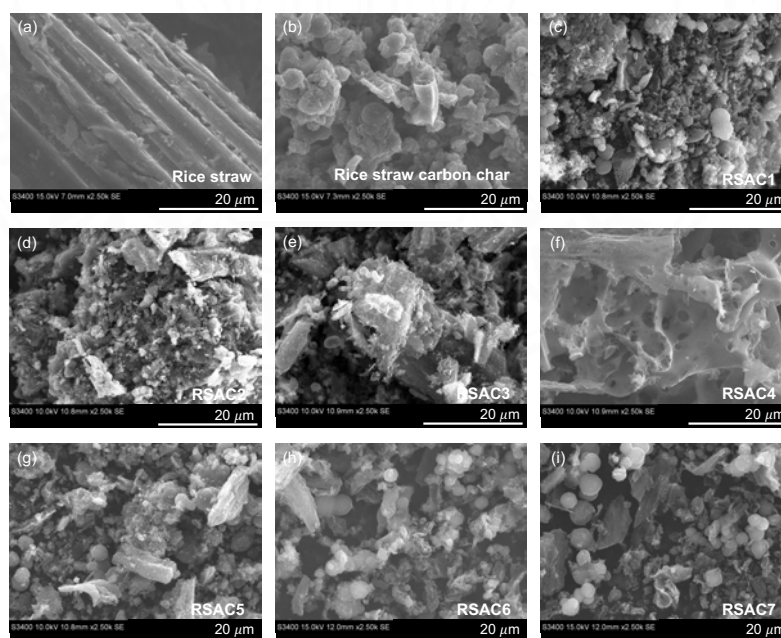
Figure 4.1 SEM images of (a) rice straw, (b) rice straw carbon char, (c) RSAC1, (d) RSAC2, (e) RSAC3, (f) RSAC4, (g) RSAC5, (h) RSAC6, and (i) RSAC7 at a magnification of 2,500X.

The SEM image of the rice straw carbon char was taken and compared with that of rice straw (Figure 4.1a and b). In addition to the different physical appearance of the rice straw carbon char as black powder as opposed to the brown straw, the SEM image of the rice straw carbon char looked very different from that of the untreated rice straw. The rice straw showed a rather smooth surface composed of fibril bundles covered under the epidermis (F.-h. Li, Hu, Yao, Wang, & Li, 2012; Xia et al., 2018) while the carbon char instead showed large spherical particles with a size of over 2 μm. This result suggests that the hydrothermal treatment successfully converted the rice straw to carbon char. The char was then mixed with KOH and then thermally activated with a continuous flow of N_2 gas. KOH was chosen as a chemical activating agent because it is widely used for producing high-quality activated carbon with enhanced microporosity as well as mesostructural order (Yu et al., 2020). Seven activating conditions were applied to investigate the effects of KOH/carbon char weight ratio, activation temperature, and activation time on the structural and electrical properties of the activated carbon (Table 3.1). After washing and drying, the activated carbon was obtained.

The effects of the KOH/carbon char weight ratio (0.5:1, 1:1, and 1:0.5 for RSAC1, RSAC2, and RSAC3, respectively) were investigated first. After chemical activation of carbon char, all three samples showed cracked and pitted morphology (Figure 4.1). However, RSAC1 and RSAC3 showed a variety of particle sizes and irregular particles whereas RSAC2 showed smaller and more regular particle sizes. RSAC1 yielded much lower surface area and pore volume, but larger pore size, compared to RSAC2 and RSAC3 (Table 4.1), indicating that the concentration of KOH was insufficient to produce microporous structures in RSAC1 (Guo, Guo, Ma, & Zhu, 2020). This means the weight ratio between KOH and carbon char is important in controlling the morphology and porosity of the activated carbon.

Table 4.1

Physical properties and specific capacitances of the RSAC.

Sample ID	Surface area ($m^2\ g^{-1}$)	Pore volume ($cm^3\ g^{-1}$)	Pore size (nm)	Mass yield (%)	Capacitance ($F\ g^{-1}$)
RSAC1	148.74	0.56	4.90	35	10
RSAC2	1004.30	0.72	3.06	26	30
RSAC3	1339.56	0.15	3.06	15	13
RSAC4	1107.26	0.13	3.82	36	2
RSAC5	1026.67	0.10	3.42	30	10
RSAC6	970.52	0.11	3.06	21	20
RSAC7	897.51	0.80	4.32	16	10

Next, the effects of the activation temperature (700, 800, and 900 °C for RSAC4, RSAC2, and RSAC5) were investigated. The SEM image of RSAC4 showed the disappearance of particles. However, RSAC2 showed small and regular particle sizes whereas RSAC5 exhibited larger rod and spherical-like particles. All three samples showed similar surface area; however, RSAC2 had a higher pore volume and lower pore size, compared to RSAC4 and RSAC5. This indicates that RSAC2 is more porous than RSAC4 and RSAC5 and the activation temperature governed the morphology and porosity of the activated carbon. The highest mass yield of RSAC4 also suggests an incomplete activation at 700 °C. Lastly, the effects of activation time (60, 90, and 120 min for RSAC2, RSAC6, and RSAC7) were examined. It was found that based on SEM images, increasing the activation time from 60 to 90 min resulted in the formation of larger particles. A further increase in activation time to 120 min did not significantly affect the morphology. From BET analysis, RSAC2 showed a larger surface area than RSAC6 and RSAC7. Long activation time might have destroyed the porous structure of the activated carbon (Hsi, Horng, Pan, & Lee, 2011). Based on all of these results, the KOH/carbon char weight ratio, activation temperature, and activation time all affected the morphology and porosity of the resulting activated carbon.

4.1.2 Electrochemical properties of RSAC

The electrochemical characterization of rice straw-derived activated carbon was investigated using a potentiostat/galvanostat. The cyclic voltammograms of RSAC1-7 were measured in conventional H_3PO_4/PVA electrolyte (Figure 4.2). It was found that RSAC2 had the highest specific capacitance of 30 F g^{-1} and a potential window of 1.6 V. According to the SEM and BET results, it can be concluded that a combination of large surface area, large pore volume, and small pore size allowed RSAC2 to accommodate electrolytes and transport ions, giving rise to its highest charge storage (Heimböckel, Hoffmann, & Fröba, 2019). RSAC4, however, yielded the lowest specific capacitance, which is consistent with the SEM image that its particulate structure formation was not completed. Based on its highest specific capacitance, RSAC2 was then chosen for subsequent experiments throughout the paper.
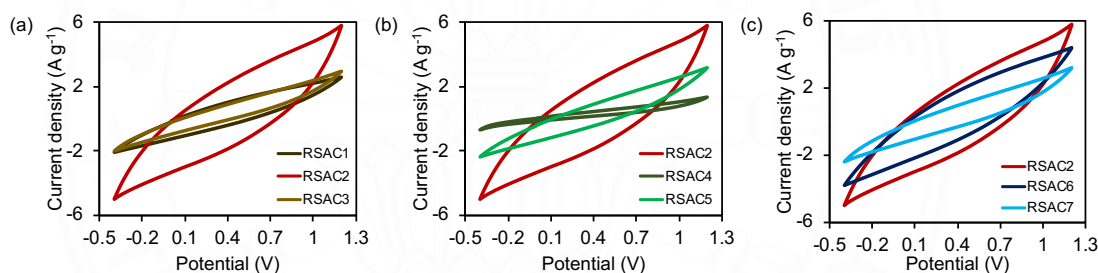
Figure 4.2 Cyclic voltammograms of RSAC prepared with different (a) KOH/carbon char weight ratio, (b) activation temperature, and (c) activation time in H_3PO_4/PVA electrolyte with a scan rate of 50 mV s^{-1}.

4.1.3 Characterizations of RSCDs

After separating RSCDs from carbon char, the RSCDs were purified by neutralization, dialysis, and freeze-drying to obtain the brown solid powder. Fourier transform infrared (FT-IR) spectroscopy and X-ray photoelectron spectroscopy (XPS) were used to identify the functional groups and chemical composition of RSCDs.
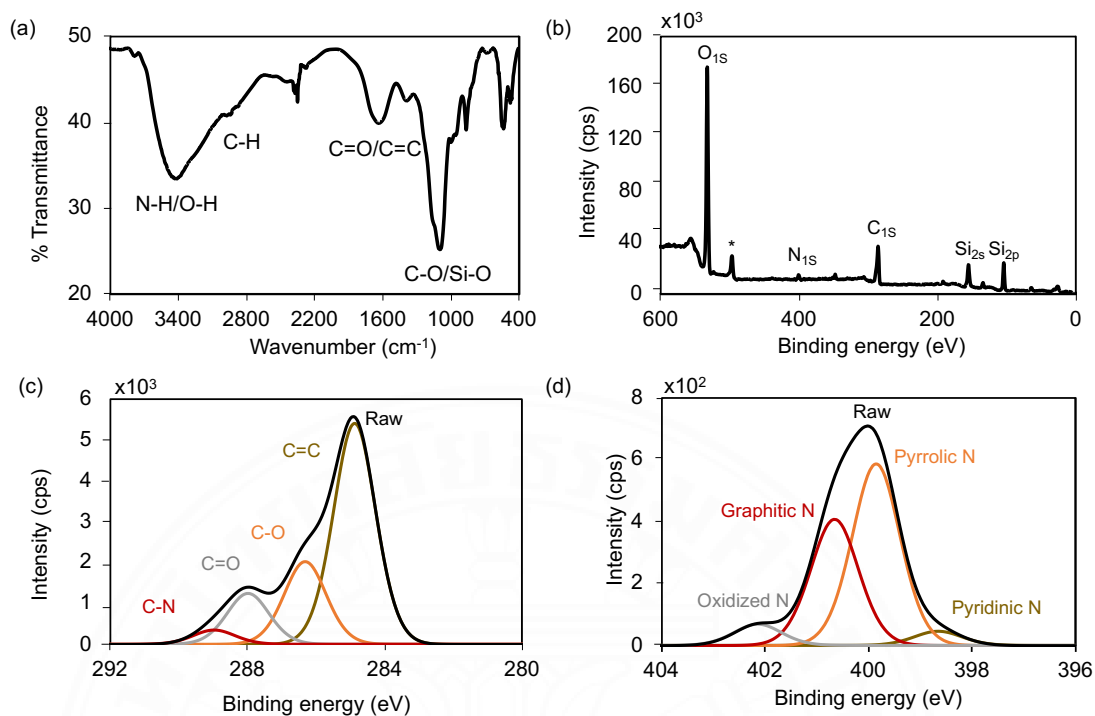
Figure 4.3 (a) FT-IR spectrum, (b) XPS survey spectrum, (c) high-resolution C_{1s} spectrum, and (d) high-resolution N_{1s} spectrum of RSCDs.

The FT-IR spectrum of RSCDs in a range of 400-4000 cm^{-1} showed signals at 3451 cm^{-1}, 2968 cm^{-1}, 1631 cm^{-1}, and 1092 cm^{-1}, corresponding to N-H/O-H stretching, C-H stretching, C=O/C=C stretching, and C-O/Si-O stretching, respectively (Figure 4.3a). The survey XPS spectrum of RSCDs (Figure 4.3b) showed major signals at 532.6 eV, 400.6 eV, 285.6 eV, and 103.6 eV, which were attributed to O_{1s}, N_{1s} C_{1s}, and Si_{2p}, with atomic concentrations of 47.19%, 2.15%, 31.90%, and 13.90%, respectively. The presence of the Si_{2p} peak is due to the fact that silica is rich in cell walls of rice straw (Thongsai et al., 2019). The high resolution of C_{1s} spectrum (Figure 4.3c) exhibited signals of C-N, C=O, C-O, and C=C at 289.2 eV, 288.2 eV, 286.5 eV and 285.1 eV, respectively. The high resolution of N1s spectrum showed pyridinic, pyrrolic, graphitic, and oxidized nitrogen at 398.7, 399.9, 400.7, and 402.2 eV, respectively (Figure 4.3d). Both FT-IR and XPS spectrum results confirmed the presence of nitrogen and oxygen-containing functional groups and expected elemental

compositions in RSCDs. These results also confirm the hydrophilicity and stable dispersion of RSCDs in aqueous solution.
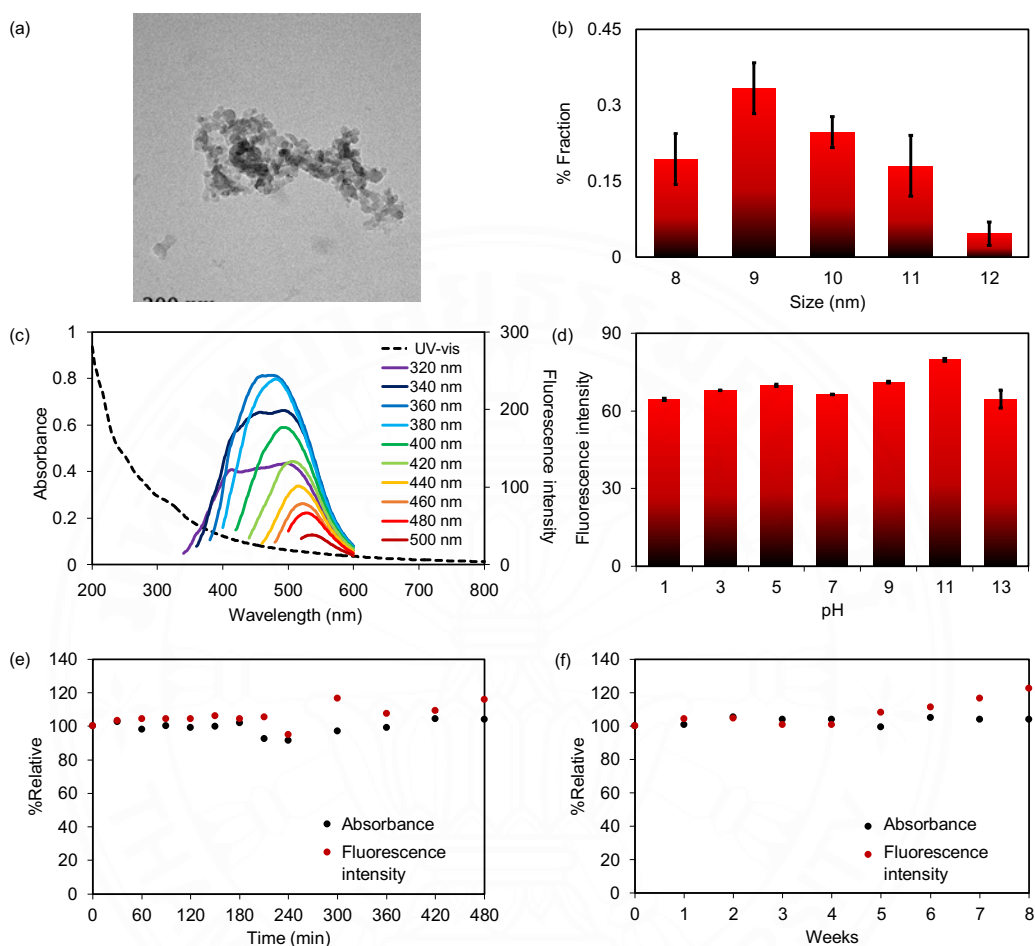
Figure 4.4 **(**a) TEM image of RSCDs and (b) size distribution of RSCDs from the TEM image. (c) UV-visible and fluorescence spectra of RSCDs at excitation wavelengths from 320 nm to 500 nm, (d) fluorescence emission intensity of RSCDs at an excitation wavelength of 345 nm in different pH, relative absorbance and fluorescence intensity of RSCDs measured (e) under UV irradiation (365 nm) and (f) under ambient conditions.

Transmission electron microscopy (TEM) was used to characterize the morphology and size of RSCDs. The RSCDs had spherical shapes and diameters ranging from about 8 to 11 nm and approximately a diameter of 9 nm on average

(Figure 4.4a and b). The zeta potential of the RSCDs was determined to be -35.6 mV, indicating the negatively charged functional groups on the surface and the stability of RSCDs (Figure 4.5).
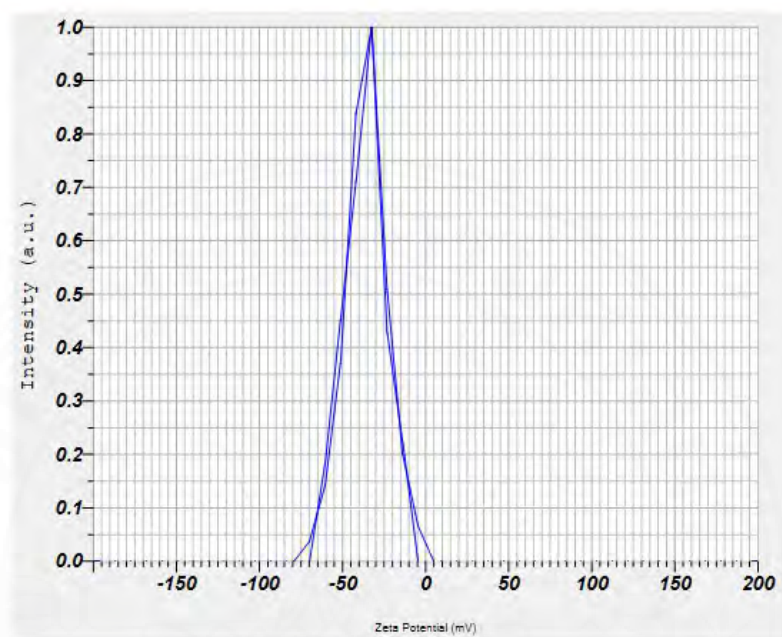
Figure 4.5 The zeta potential graph of RSCDs.

UV-visible spectroscopy and fluorescence spectroscopy were used to characterize the optical properties of RSCDs. The UV-visible spectrum of RSCDs (Figure 4.4c) shows the absorption band ranging from 200 to 600 nm. Small peaks at 250 and 320 nm corresponded to the π-π^* transition of the aromatic sp^2 and n-π^* transition of the C=O bonds, respectively. The fluorescence spectra with excitation wavelengths from 320 to 500 nm were obtained. An excitation wavelength of 345 nm showed a maximum emission intensity at an emission wavelength of 440 nm. The fluorescence spectra display excitation-dependent characteristics, attributed to the distribution of particle sizes and various emissive sites of RSCDs. Fluorescence emission intensity of RSCDs at an excitation wavelength of 345 nm was investigated from pH 1 to 13. It was found that fluorescence emission of RSCDs was not significantly altered by pH (Figure 4.4d). The photostability of RSCDs was next

investigated by measuring the UV-vis absorbance and fluorescence emission under 365-nm UV irradiation and ambient conditions (Figure 4.4e and f). It was found that the photostability of the RSCDs was relatively stable under both UV irradiation for at least 8 h and ambient conditions for at least 8 weeks. This indicates that the RSCDs are stable for long-term use and application.

4.1.4 Electrical properties of rice-based electrolytes

For a high energy-density supercapacitor, not only specific capacitance but also the potential window is important. In this study, the electrolyte was fabricated from rice and H_3PO_4 and compared to H_3PO_4/PVA electrolyte and the electrode was made from RSAC2. Upon mixing, the acidified rice became gel-like and highly viscous due to the solvation effects between ionic species and polysaccharides.
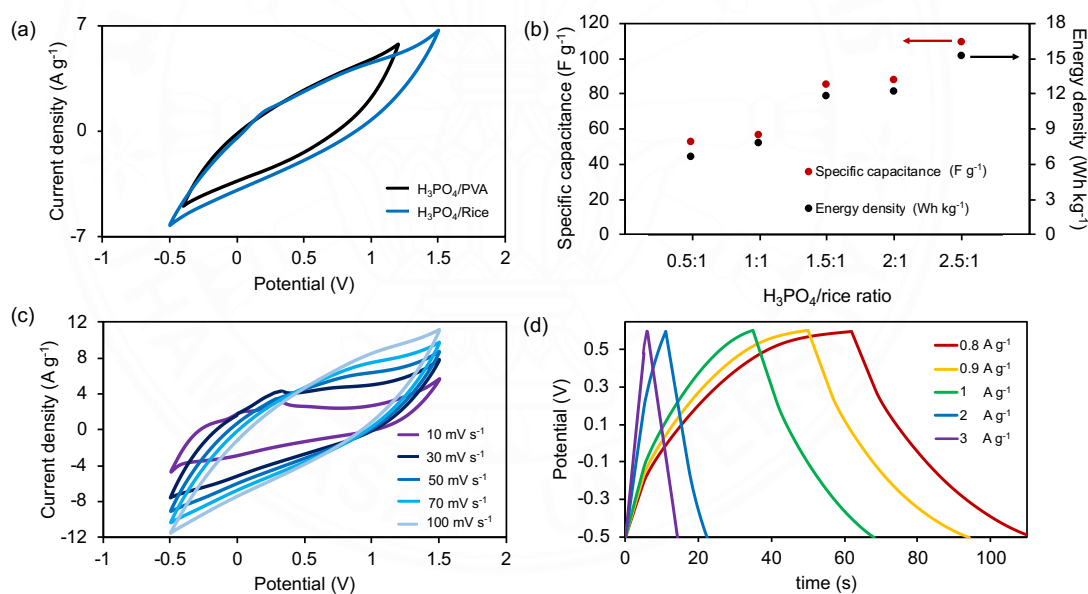
Figure 4.6 Cyclic voltammograms of RSAC2 in (a) 1:1 H_3PO_4/PVA and 1:1 H_3PO_4/rice electrolyte at a scan rate of 30 mV s^{-1}, (b) H_3PO_4/rice electrolyte with different concentrations of H_3PO_4 at a scan rate of 30 mV s^{-1}, and (c) 2:1 H_3PO_4/rice electrolyte at different scan rates. (d) GCD curves of RSAC2 in 2:1 H_3PO_4/rice electrolyte at different current densities.

The electrical properties were measured using cyclic voltammetry in a three-electrode system. As shown in Figure 4.6a, the cyclic voltammogram from H_3PO_4/rice electrolyte was slightly larger than that that from H_3PO_4/PVA electrolyte, giving a specific capacitance of 56 vs 45 F g^{-1}, which is equivalent to a 124% enhancement. The H_3PO_4/rice electrolyte exhibited a 2.0 V potential window, which is higher than the H_3PO_4/PVA electrolyte by 0.4 V. The corresponding energy density of H_3PO_4/rice and H_3PO_4/PVA electrolytes are 8 and 4 Wh kg^{-1}, equivalent to a 200% increase. As a result, the H_3PO_4/rice electrolyte is a promising alternative polymer electrolyte as it gave better electrical performance and is cheaper than the PVA, a conventional polymer for electrolyte. The highly solvating properties of rice led to the enhanced performance.

Table 4.2

The electrical properties of RSAC2 electrode in different ratios of H_3PO_4/rice electrolyte.

Polymer	H_3PO_4:polymer (w/w)	Voltage (V)	Specific capacitance (F g^{-1})	Energy density (Wh kg^{-1})
PVA	1:1	1.6	45	4
Rice	0.5:1	1.9	52	7
Rice	1:1	2.0	56	8
Rice	1.5:1	2.0	85	12
Rice	2:1	2.0	88	12
Rice	2.5:1	2.0	109	15

Next, to investigate the effects of H_3PO_4, the ratio between H_3PO_4 and rice was varied. Using 0.5:1 H_3PO_4/rice, the potential window, specific capacitance, and energy density of 1.9 V, 52 F g^{-1}, and 7 Wh kg^{-1} (Table 4.2) were obtained. Upon increasing the ratio to 2.5:1 H_3PO_4/rice, the potential window and specific capacitance increased to 2.0 V and 109 F g^{-1}, equivalent to an energy density of 15 Wh kg^{-1}. This suggests that an improvement of electrical properties is due to an

increase in ionic conductivity of the electrolyte. Nonetheless, all tested concentrations of H_3PO_4/rice even at 0.5:1 provided better electrical performance than the H_3PO_4/PVA electrolyte. For subsequent experiments, the 2:1 H_3PO_4/rice electrolyte was used because it produced excellent electrical properties and still had a gel-like appearance.

The CV and GCD of RSAC2 in 2:1 H_3PO_4/rice electrolyte were measured at scan rates from 10 mV s^{-1} to 100 mV s^{-1} and applied current densities from 0.8 A g^{-1} to 3 A g^{-1}, respectively. The CV profile indicates that the peak current increased when the scan rate was increased (Figure 4.6c). However, increasing the scan rate decreased the specific capacitance from 162 to 30 F g^{-1}. The scan rate-dependence capacitance confirmed the diffusion-controlled process of electrolyte. The capacitance of the supercapacitor is enhanced when electrolyte can effectively diffuse through the micro and mesoporous surfaces. A low scan rate allows the electrolyte to diffuse through the micro and mesoporous surfaces, and therefore, the specific capacitance will be significantly enhanced. On the other hand, a high scan rate allows the electrolyte to access only the mesoporous surface, and specific capacitance is therefore suppressed (Daraghmeh et al., 2017). The GCD profile also showed consistent results with CV results, in which increasing the current rate decreased specific capacitance (Figure 4.6d). The GCD curves, especially at high current rates, were almost symmetrical, indicating a reversible charge-discharge cycle.

4.1.5 CDs as electrolyte additives

It has been reported that an addition of some redox active species or electro-active molecules to electrolytes can enhance the overall electrical performance (Senthilkumar, Selvan, & Melo, 2013). CDs have been reported to enhance performance of various electronic and optoelectronic applications, including solar cells (Ghann et al., 2019; Rezaei, Irannejad, Ensafi, & Kazemifard, 2019), sensors (Kumari & Chaudhary, 2020; Wen et al., 2020), batteries (Jiang et al., 2020; S. Wang et al., 2018), light-emitting diodes (L. Jin et al., 2020; Zhao et al., 2019), fuel cells (Mohideen, Liu, & Ramakrishna, 2020), photocatalysts (Prasannan & Imae, 2013), etc. The use of CDs in supercapacitor electrodes has been also found to enhance the performance (Kumar et al., 2016). However, their uses as additives in supercapacitor electrolytes have never been reported.
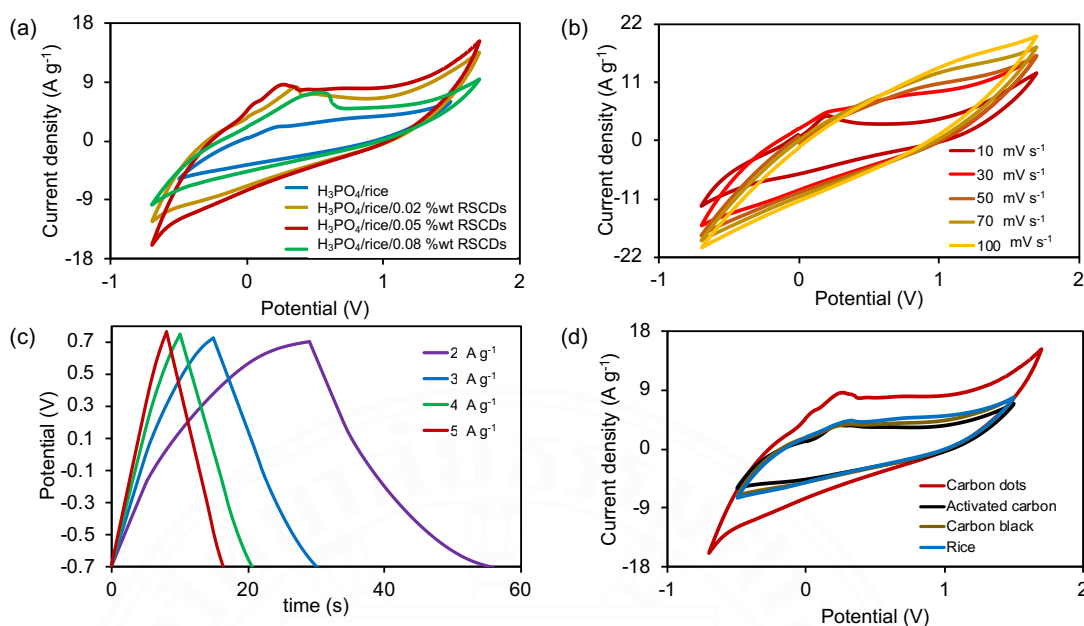
Figure 4.7 Cyclic voltammograms of RSAC2 in (a) H_3PO_4/rice electrolyte and H_3PO_4/rice/RSCDs electrolyte with different concentrations at a scan rate of 30 mV s^{-1} and (b) H_3PO_4/rice/0.05%wt RSCDs electrolyte at different scan rates. (c) GCD of RSAC2 in H_3PO_4/rice/0.05%wt RSCDs electrolyte at different current densities (d) Cyclic voltammograms of RSAC2 in H_3PO_4/rice electrolyte in the absence and presence of different carbon materials.

Table 4.3

The electrical properties of RSAC2 electrode in various electrolytes.

Electrolyte	Potential window (V)	Specific capacitance (F g^{-1})	Energy density (Wh kg^{-1})
H_3PO_4/rice	2.0	88	12
H_3PO_4/rice/0.02%wt RSCDs	2.4	128	26
H_3PO_4/rice/0.05%wt RSCDs	2.4	144	29
H_3PO_4/rice/0.08%wt RSCDs	2.4	87	17
H_3PO_4/rice/0.05%wt AC	2.0	75	10
H_3PO_4/rice/0.05%wt CB	2.0	83	12

*AC = activated carbon and CB = carbon black

In this experiment, the RSCDs were then added to the H_3PO_4/rice electrolytes. Figure 4.7a shows cyclic voltammograms of H_3PO_4/rice electrolyte and H_3PO_4/rice electrolytes in the presence of RSCDs at different concentrations. The 2:1 H_3PO_4/rice electrolyte provides a potential window, specific capacitance, and energy density of 2.0 V, 88 F g^{-1}, and 12 Wh kg^{-1}, respectively. In contrast, all H_3PO_4/rice electrolytes in the presence of RSCDs concentrations give 2.4 V (Table 4.3). The specific capacitance and energy density of H_3PO_4/rice electrolyte with the presence of 0.02 %wt RSCDs are 128 F g^{-1} and 26 Wh kg^{-1}, respectively and further increased to 144 F g^{-1} and 29 Wh kg^{-1}, 2.4 times higher than the H_3PO_4/rice electrolyte, when using 0.05 %wt RSCDs. However, when increasing the concentration of RSCDs to 0.08 %wt, the specific capacitance dropped but the energy density was still higher than the pristine H_3PO_4/rice electrolyte. The current response is again a scan rate dependence (Figure 4.7b). The highest specific capacitance of 491 F g^{-1} was obtained at the scan rate at 2 mV s^{-1}. We further investigated the effects of other types of carbon materials as additives in H_3PO_4/rice electrolyte, including our rice straw-derived activated carbon (AC) and carbon black (CB). Unlike the RSCDs, both AC and CB did not provide a significant improvement of specific capacitance and energy density as compared to the pristine H_3PO_4/rice electrolyte (Figure 4.7d and Table 4.3). This suggests the contribution of small size, abundant functional groups, and hydrophilicity of RSCDs to the improvement in supercapacitor performance.

The Nyquist plots of the supercapacitors were obtained (Figure 4.8a). The series resistances of RSAC2 electrode in H_3PO_4/rice electrolyte, H_3PO_4/rice electrolyte with RSCDs, AC, and CB are 12.6, 7.7, 9.5, and 11.4 Ω, respectively, indicating all of the carbon materials reduced the series resistance when compared with the original H_3PO_4/rice electrolyte. It is obvious that the series resistance was the lowest when adding RSCDs to the electrolyte, which explains the highest specific capacitance obtained from the RSCD-containing electrolyte. Furthermore, at a high frequency region, a nearly vertical line of the CD-containing electrolyte indicates good EDLC properties. Upon bending from 0° to 180°, the specific capacitances retained appreciably well (Figure 4.8b and c). This result confirmed good electrical contacts within the electrode and between electrode and electrolyte and indicates the potential of our supercapacitors for flexible and wearable applications.
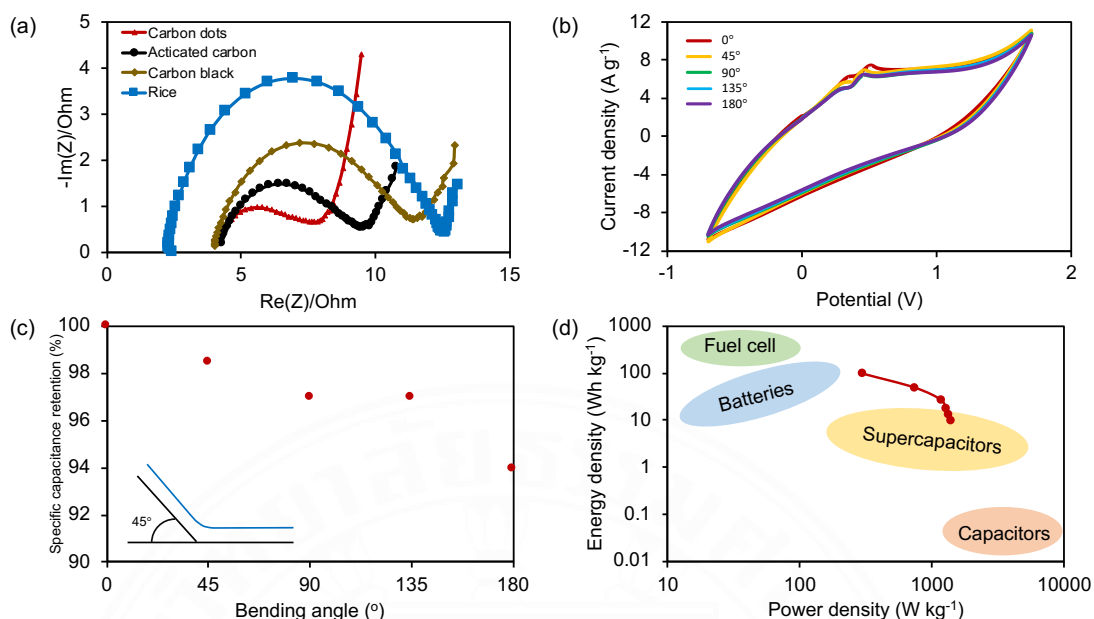
Figure 4.8 (a) Nyquist plots of RSAC2 in H_3PO_4/rice electrolyte in the absence and presence of different carbon materials. (b) Cyclic voltammograms of RSAC2 in H_3PO_4/rice electrolyte with RSCDs at bending angles of $0°$, $45°$, $90°$, $135°$, and $180°$ at a scan rate 50 mV s^{-1} and (c) specific capacitance retention. (d) Ragone plot of RSAC2 electrode in H_3PO_4/rice electrolyte with RSCDs (calculated from 2 to 100 mV s^{-1}).

As shown in Figure 4.8d and Table 4.4, the highest specific capacitance reached 491 F g^{-1} and 98 Wh kg^{-1} at a scan rate of 2 mV s^{-1}. It is clear that the energy density of our supercapacitor of 98 Wh kg^{-1} is the highest among other reported rice straw-derived supercapacitors. It is also on a par with battery counterparts (Ashritha & Hareesh, 2020). Comparing with supercapacitors fabricated from activated carbon derived from rice straw or those that used polysaccharide-based electrolytes in other reports, the obtained energy density of our supercapacitor is the highest (Table 4.4). This is due to a combination of a wide potential window and high specific capacitance. It is noteworthy to point out that our electrode was prepared from only activated carbon and PVDF binder without an addition of highly conductive carbon like carbon black or acetylene black, which were generally used for the previously reported supercapacitors. We believe that the unique characteristics of CDs with nanometer size, surface functional groups, and extraordinary hydrophilicity possibly provided electro-

active properties and improved accessibility and wettability between electrode and electrolyte to enhance the electrical performance of the supercapacitors.

Table 4.4

Electrochemical performance of rice waste-derived activated carbon and starch-based electrolytes.

Electrode	Electrolyte	Potential window (V)	Specific capacitance ($F\ g^{-1}$)	Energy density ($Wh\ kg^{-1}$)	References
Rice straw (AC)	H_3PO_4/rice/0.05 %wt RSCDs	2.4	491 (2 mV s^{-1})	98	This work
Rice straw (AC)	1 M H_2SO_4	0.8	357 (0.5 A g^{-1})	29.3	(Chen et al., 2018)
Rice straw (AC)	([EMIM][BF$_4$])	2.5	80 (0.1 A g^{-1})	17.4	(Sudhan et al., 2017)
Rice straw (AC)	6 M KOH	1.0	400 (0.1 A g^{-1})	13.9	(H. Jin et al., 2018)
Rice straw (AC)	6 M KOH	1.0	420 (1 A g^{-1})	11.1	(G. Zhou et al., 2020)
Rice straw (AC)	0.5 M H_2SO_4	1.0	93 (10 mV s^{-1})	-	(Nam et al., 2018)
AC	Powdered neem gum in LiBF$_4$	2.0	640 (0.5 A g^{-1})	22.2	(Dhar et al., 2020)
AC	CMC blended with K-carrageenan and doped with NH$_4$NO$_3$	1.0	25.83 (2 mV s^{-1})	-	(Zainuddin et al., 2020)
AC	CS:MC:NH$_4$SCN	0.9	76.7 (10 mV s^{-1})	8.63	(Aziz et al., 2019)

4.1.6 Analysis of electron transfer

To further investigate the effects of the CDs on the enhanced specific capacitance, the electron transfer process was analyzed from the CV profiles. Two systems, H_3PO_4/rice and H_3PO_4/rice/0.05 %wt RSCDs electrolytes, were examined. The Cottrell's equations (Equation 4.1 and 4.2) can be used to provide an information on the electron transfer process whether it is the diffusion-controlled, surface-controlled (adsorption) process, or a combination of both (L. Li, Zhang, Zhang, Zhang, & Zhang, 2019).

$$i = av^b \qquad \text{(Equation 4.1)}$$

$$\log i = \log a + b \log v \qquad \text{(Equation 4.2)}$$

where i is the current response, v is the scan rate, a and b are variable parameters. When the b value, obtained from the slope, is 0.5, the charge transfer is the diffusion-controlled process. However, if the b value is 1, it is instead the surface-controlled process. As shown in Figure 4.9a, in the absence of RSCDs the charge transfer in H_3PO_4/rice electrolyte was predominantly the diffusion-controlled process ($b = 0.610$). An addition of the RSCDs to the H_3PO_4/rice electrolyte, however, increased the b value from 0.610 to 0.746, indicating that the CDs improved the surface-controlled process of charge transfer. A b value of 0.746 also confirms that both diffusion- and surface-controlled processes virtually equally contributed to the charge transfer. A contribution from both surface- and diffusion-controlled processes might synergistically lead to optimum charge transfer efficiency. To further confirm this finding, the adsorption equation (Equation 4.3) (Supchocksoonthorn, Thongsai, Wei, Gopalan, & Paoprasert, 2021) and Randles-Sevcik's diffusion equation (Equation 4.4) (Aristov & Habekost, 2015) were used to further analyze the charge transfer process.

$$i = \frac{n^2 F^2}{4RT} vA\Gamma \qquad \text{(Equation 4.3)}$$

$$i = 0.436nFAC^0 \left(\frac{nFvD_0}{RT}\right)^{\frac{1}{2}} \qquad \text{(Equation 4.4)}$$

where n is the number of transferred electrons (mol), F is the Faraday's constant (96,485 C mol^{-1}), R is the universal gas constant (8.314 J mol^{-1} K^{-1}), T is the temperature (298 K), A is the electrode surface (cm^2), Γ is the surface coverage of the adsorbed species (mol cm^{-2}), C^0 is the bulk concentration of the electroactive species (mol cm^{-3}), and D_0 is the diffusion coefficient of the electroactive species (cm^2 s^{-1}). The plot of current response vs scan rate (v) (Figure 4.9b) was constructed based on Equation 4.3 whereas the plot of current response vs the square root of scan rate ($v^{1/2}$) (Figure 4.9c) was made following Equation 4.4. It was found that both plots for the H$_3$PO$_4$/rice/0.05 %wt RSCDs and H$_3$PO$_4$/rice electrolytes gave high coefficients of determination (R^2). Therefore, it can be concluded that both adsorption- and diffusion-controlled processes contributed to the charge transfer. Interestingly, it is obvious that the slopes of H$_3$PO$_4$/rice/0.05%wt RSCDs from both plots are higher than those of H$_3$PO$_4$/rice. This verifies that the addition of CDs in electrolyte enhanced key parameters, such as number of transferred electrons (n), surface coverage of the adsorbed species (Γ) and/or diffusion coefficient of the electroactive species (D_0), as these are parts of the slopes. Although there was insufficient data to determine which parameter(s) dominantly or partly contributed to the charge transfer process, it is enough to conclude that the CDs led to a distinct improvement in several factors for charge transfer via diffusion and adsorption processes, which in turn reduced the series resistance and enhanced the supercapacitor performance.
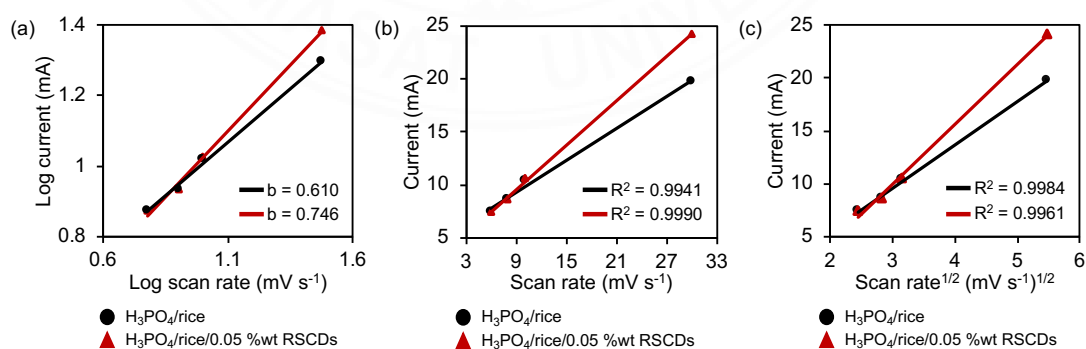

Figure 4.9 The plot (a) log i vs log v, (b) i vs v, and (c) i vs v$^{1/2}$ of RSAC2 electrode in H$_3$PO$_4$/rice and H$_3$PO$_4$/rice/0.05 %wt RSCDs electrolytes at 1 V.

4.1.7 Analysis of capacitance

As the CV curves are quasi-rectangular in shape, our supercapacitors are not totally EDL capacitors. Pseudocapacitance also contributed to the specific capacitance. For further investigation, the Dunn's method was used to examine the contribution from surface capacitance (EDL) and pseudocapacitance (diffusion) (J. Liu et al., 2018; Shao et al., 2015). The relationship between current response ($i(v)$) at a fixed potential and scan rate is shown in Equation 4.5 and 4.6.

$$i(v) = k_1 v + k_2 v^{1/2} \qquad \text{(Equation 4.5)}$$

$$\frac{i(v)}{v^{1/2}} = k_1 v^{1/2} + k_2 \qquad \text{(Equation 4.6)}$$

where k_1 and k_2 are the surface capacitive and diffusion coefficients, which can be then obtained from the slope and intercept from the $\frac{i(v)}{v^{1/2}}$ vs $v^{1/2}$ plot, respectively. As shown in Figure 4.10a, upon the addition of RSCDs, the contribution from surface capacitance became more pronounced at all scan rates, consistent with analysis using the Cottrell's equations in which the CD increased the surface-controlled process. At a scan rate of 30 mV s^{-1}, the surface capacitance in the H_3PO_4/rice/0.05 %wt RSCDs electrolyte system dominantly contributes 69% (Figure 4.10c), as compared to only 28% in the H_3PO_4/rice system (Figure 4.10b). It can be concluded that 1) the CDs improved the surface capacitance contribution, 2) both surface- and diffusion-controlled capacitances played an important role in controlling the supercapacitor performance, and 3) the CDs synergistically led to optimal contribution of both surface and diffusion processes. We believe that the unique characteristics of CDs with nanometer size, surface functional groups, and extraordinary hydrophilicity possibly provided electro-active properties and improved accessibility and wettability between electrode and electrolyte to enhance surface adsorption and diffusion of ions and to reduce the series resistance, thereby leading to the enhanced electrical performance of the supercapacitors (Figure 4.10d).
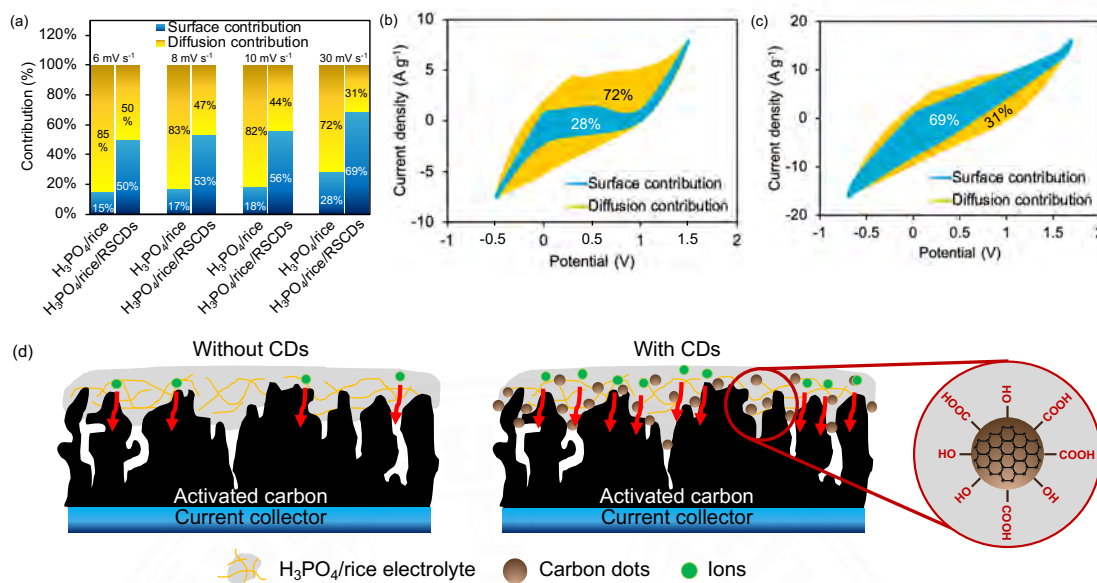
Figure 4.10 (a) Comparison of surface capacitive and diffusion contributions of RSAC2 electrode in H_3PO_4/rice and H_3PO_4/rice/0.05 %wt RSCDs electrolytes at different scan rates. CV plots of RSAC2 electrode in (b) H_3PO_4/rice and (c) H_3PO_4/rice/0.05 %wt RSCDs electrolyte at a scan rate of 30 mV s^{-1}. (d) Schematic of electrolytic ion accessibility of an electrode in (left) H_3PO_4/rice electrolyte and (right) H_3PO_4/rice/RSCDs electrolyte.

4.1.8 Stability

Next, the recyclability of our supercapacitor was investigated. It was found that the specific capacitance did not decrease for 1,000 cycles and then slowly dropped to 84% after 5,000 cycles (Figure 4.11a). We also investigated with the shelf life of our H_3PO_4/rice/0.05 %wt RSCDs electrolyte. Photos of electrolytes were taken and CV were measured over a period of 8 weeks (Figure 4.11b). The photos showed no changes of the electrolytes (Figure 4.11c). The specific capacitance did not significantly vary as a function of time. Moreover, phosphoric acid was reported that it obviously presented higher antimicrobial activity especially in gram-positive bacteria (Arias-Moliz, Ferrer-Luque, Espigares-Rodríguez, Liébana-Ureña, & Espigares-García, 2008; Prado et al., 2015). We believed that phosphoric acid acted as a preservative to prevent rice from spoiling. These results confirm that our supercapacitor

can be used for several thousand cycles and a long period of time, which will be sufficient for practical applications.
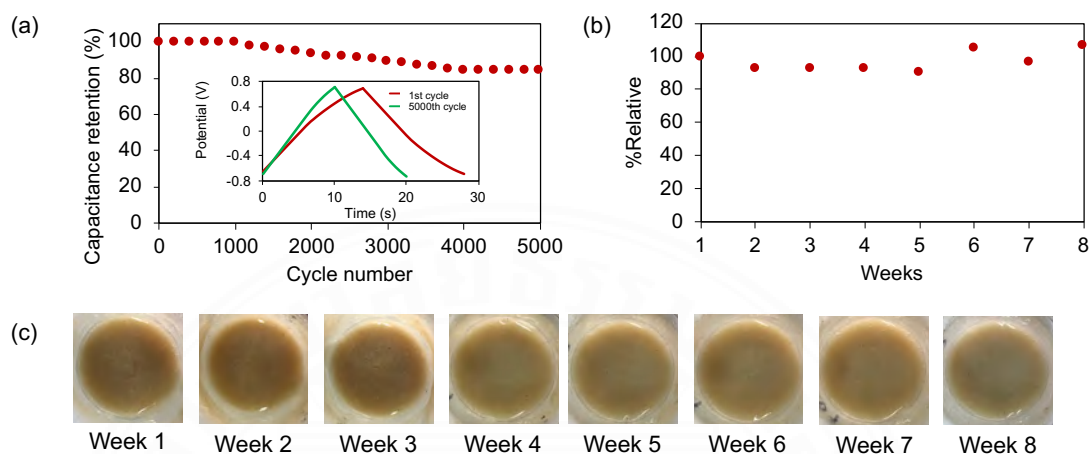
Figure 4.11 (a) Recyclability of RSAC2 electrode in H_3PO_4/rice/0.05 %wt RSCDs electrolyte up to 5,000 cycles at a current density of 3 A g^{-1} (inset Figure show the GCD curves at 1st and $5,000^{th}$ cycles), (b) relative specific capacitances of RSAC2 electrode in H_3PO_4/rice/0.05 %wt RSCDs electrolyte, and (c) photos of electrolytes measured for 8 weeks.

4.2 Synthesis, characterization, and application of activated carbon and carbon dots from rice husk

4.2.1 Synthesis and characterization of RHAC

Rice husk is one of the abundant agricultural wastes after rice harvesting. Rice husk is rich in carbon content because it is lignocellulosic biomass which consists of three main components, including cellulose, hemicellulose, and lignin. In this work, AC and CDs were simultaneously synthesized from rice husk in a two-in-one approach. The carbon char was obtained from the filtered residue whereas the carbon dots were obtained from the filtrate. The carbon char was activated to produce activated carbon via pyrolysis and the purified CDs were used as additives in an electrode as composite materials. In this work, RHAC and RHCDs refer to rice husk activated carbon and rice husk carbon dots, respectively.

As shown in Figure 4.12a, the SEM image of rice husk carbon char shows that the carbon char mostly comprised particles. On the other hand, Figure 4.12b exhibits the physical appearance of RHAC with a mixture between small pieces and particles.
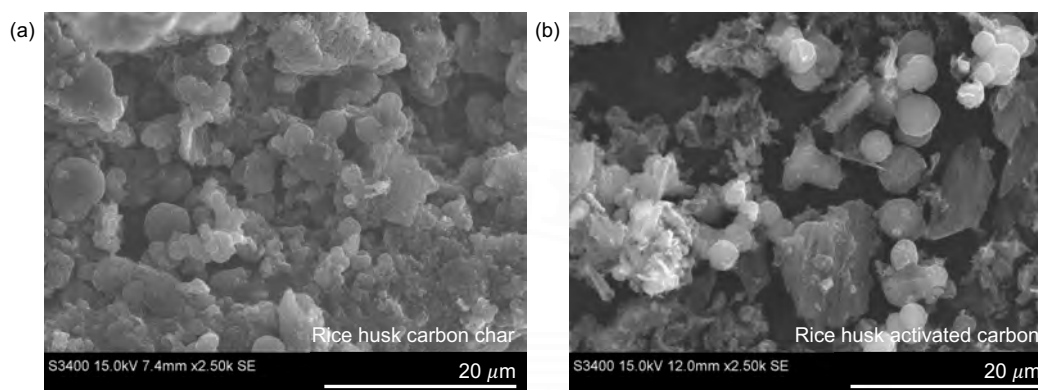
Figure 4.12 SEM images of (a) rice husk carbon char and (b) RHAC at a magnification of 2,500X.

4.2.2 Characterization of RHCDs

The functional groups and elemental components of RHCDs were analyzed by using Fourier-transform infrared spectroscopy and X-ray photoelectron spectroscopy, respectively. As shown in Figure 4.13a, the FT-IR spectrum of RHCDs in a range of 400-4000 cm^{-1} shows diverse functional groups on their surfaces, such as a broad signal of hydroxyl (3200-3500 cm^{-1}) and a sharp signal of the carbonyl group (1591 cm^{-1}). Since rice husk is rich in silica, the Si-O signal shows up at around 1390 cm^{-1}. The XPS survey spectrum of RHCDs (Figure 4.13b) shows signals at 532.0 eV, 400.0 eV, 285.0 eV, and 103.0 eV which corresponded to O_{1s}, N_{1s}, C_{1s}, and Si_{2p} with atomic concentrations of 26.30%, 4.49%, 62.67%, and 2.19%, respectively. The high-resolution of RHC_{1s} spectrum of CDs (Figure 4.13c) displays signals of C=C, C-O, C=O, and C-N at 285.03 eV, 286.47 eV, 288.33 eV, and 289.34 eV, respectively. The high-resolution of N_{1s} spectrum of RHCDs (Figure 4.13d) exhibits signals of pyridinic nitrogen, pyrrolic nitrogen, and graphitic nitrogen at 399.43 eV, 400.28 eV, and 401.97 eV, respectively. Both FT-IR and XPS spectrum results confirmed the presence of

nitrogen- and oxygen-containing functional groups and the expected elemental compositions in RHCDs. These groups resulted in a good water solubility of RHCDs.
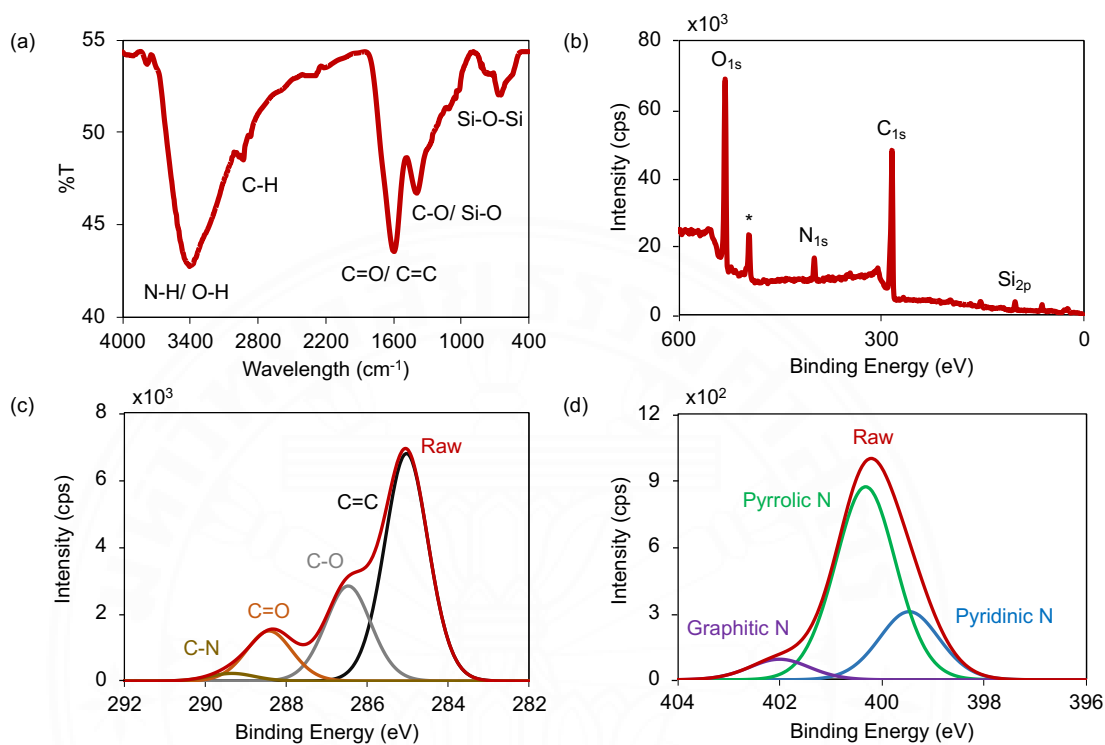
Figure 4.13 (a) FT-IR spectrum, (b) XPS survey spectrum, (c) high-resolution of C_{1s} spectrum, and (d) high-resolution N_{1s} spectrum of RHCDs.

The TEM image of RHCDs (Figure 4.14a) shows an aggregated morphology of RHCDs which corresponding to the zeta potential result as shown in Figure 4.14b, the zeta potential of the RHCDs is -22.4 mV, indicating the instable behavior of RHCDs and negatively charged functional groups on the surface of RHCDs. The RHCDs had a spherical shape with an average size of 34 nm. The UV-visible absorbance and fluorescence emission spectra of RHCDs were analyzed to determine the optical properties of RHCDs. As shown in Figure 4.14c, the UV-vis absorbance in a range of 200-800 nm shows a small peak at 260 nm, which is corresponding to the n-π* transition of the C=O bonds. The fluorescence emission spectrum of RHCDs shows the maximum fluorescence emission at 454 nm when an

excitation at 360 nm and the fluorescence emission also shifted to a higher wavelength when the excitation wavelength was increased, indicating that RHCDs are excitation-dependent due to the different sizes of RHCDs and various emissive sites on their structure.

Figure 4.14 (a) TEM image of RHCDs, (b) zeta potential graph of RHCDs, and (c) UV-visible absorbance and fluorescence spectra of RHCDs.

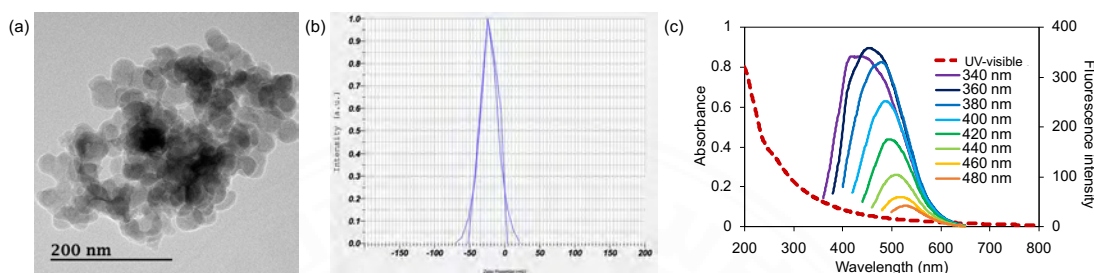### 4.2.3 Electrochemical properties

The electrochemical properties of the supercapacitor were analyzed by using cyclic voltammetry and galvanostatic charge-discharge. Figure 4.15a shows the cyclic voltammograms of RHAC electrode and RHAC/RHCDs electrode in 6 M KOH at a scan rate of 10 mV s^{-1}. The RHAC/RHCDs electrode gave a larger cyclic voltammogram than the RHAC electrode, corresponding to the specific capacitances of 109 F g^{-1} and 86 F g^{-1}, respectively. The increase in specific capacitance also led to an increase in energy density from 3.0 Wh kg^{-1} of the RHAC electrode to 3.8 Wh kg^{-1} of the AC/CDs electrode. Comparing the GCD curves between RHAC electrode and RHAC/RHCDs electrode in 6 M KOH at a current density of 1 A g^{-1} (Figure 4.15b), the RHAC/RHCDs electrode yielded a higher specific capacitance of 129 F g^{-1} while the RHAC electrode provided a specific capacitance of 104 F g^{-1} and the energy density increased from 3.6 Wh kg^{-1} of the RHAC electrode to 4.8 Wh kg^{-1} of the RHAC/RHCDs electrode. This indicates that the addition of RHCDs to RHAC in electrode improved the specific capacitance and energy density by 124% and 133%, respectively. Moreover, the RHAC electrode with the RHCDs showed a smaller IR drop (0.2 V)

when compared with an IR drop of the RHAC electrode (0.3 V). From these results, it is clear than RHCDs improved the performance of the AC-based supercapacitors.

The effects of scan rate and current density on the electrochemical performance of RHAC/RHCDs electrode were studied. Figure 4.15c shows the cyclic voltammograms of RHAC/RHCDs electrode in 6 M KOH with the scan rates of 10 to 30, 50, 70, and 100 mV s^{-1}. The specific capacitance decreased from 109 to 56, 33, 25, and 20 F g^{-1}, respectively. For the RHAC/RHCDs electrode in 6 M KOH (Figure 4.15d), increasing the current density from 0.5 to 1, 2, 3, and 4 A g^{-1} decreased the specific capacitances from 159 to 129, 91, 62, and 39 F g^{-1}, respectively. The recyclability of RHAC/RHCDs electrode was next investigated. After 100 cycles, the specific capacitance decreased only by 6.6% (Figure 4.15e). The inset displayed that the IR drop did not significantly increase after 100 cycles. This indicates a good stability of the electrode and supercapacitor, which will be suitable for long-lasting applications. The Ragone plot (Figure 4.15f) shows the highest energy density of 39.1 Wh kg^{-1} at a power density of 228.6 W kg^{-1}.
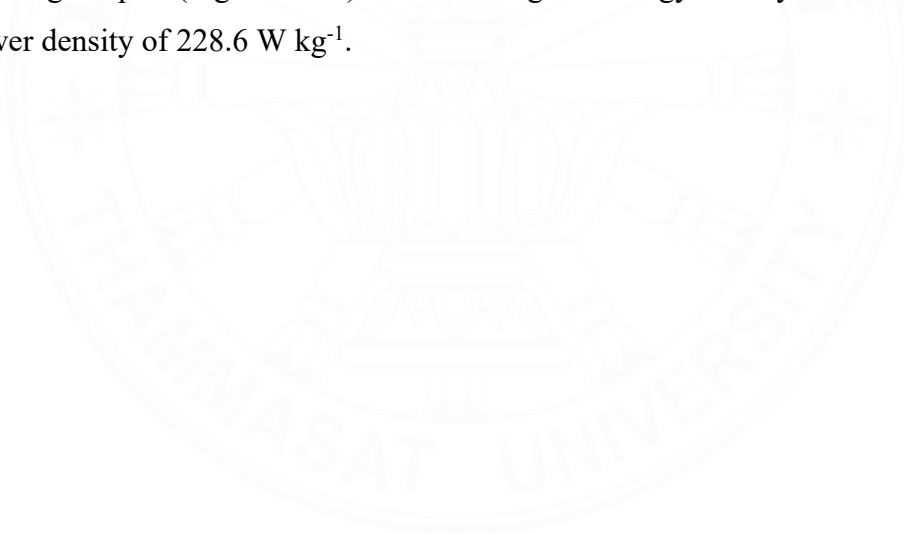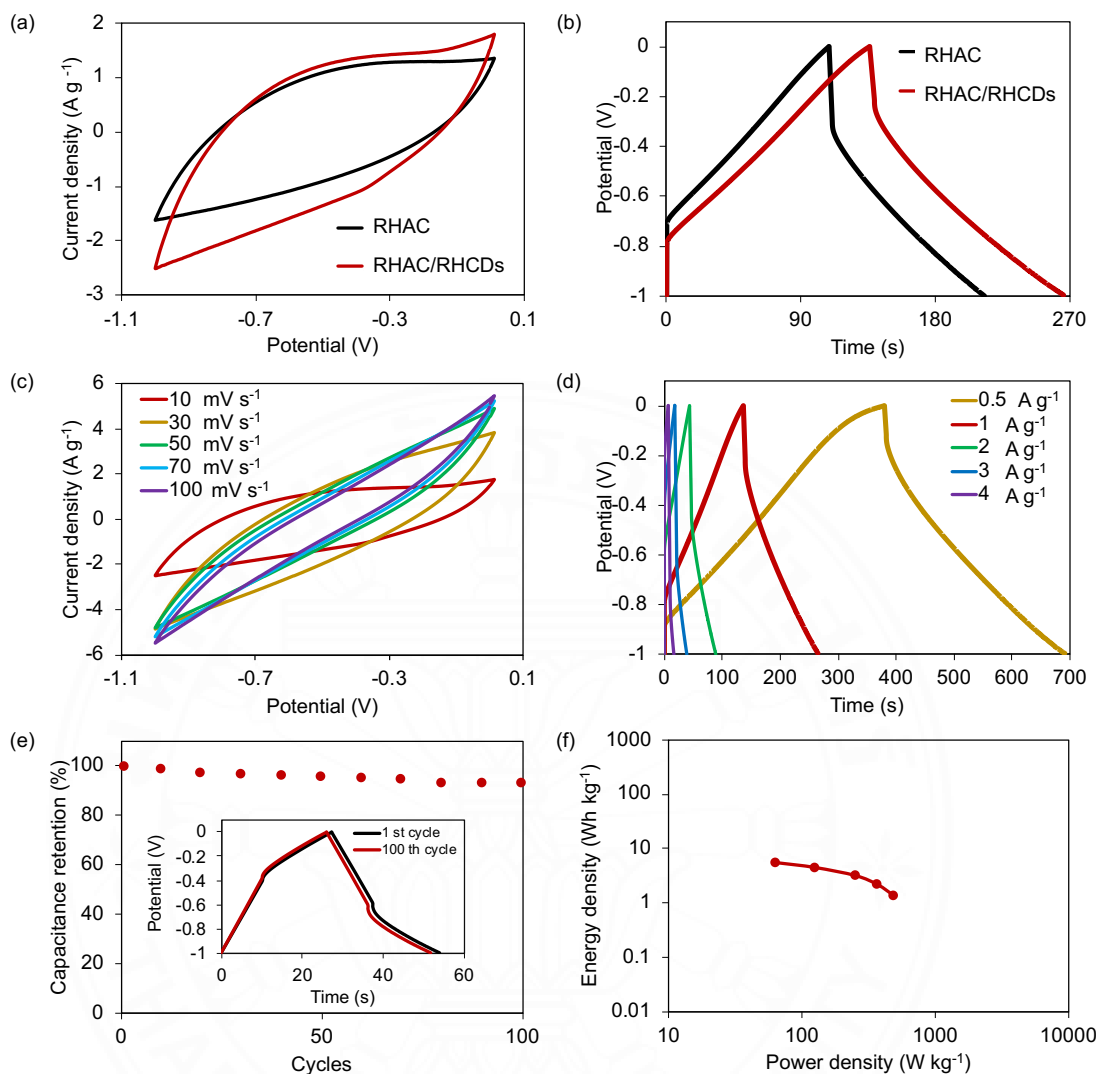
Figure 4.15 (a) Cyclic voltammograms of RHAC and RHAC/RHCDs electrodes at a scan rate of 10 mV s^{-1}, (b) GCD curves of RHAC and RHAC/RHCDs electrodes at a current density of 1 A g^{-1}, (c) cyclic voltammograms of RHAC/RHCDs electrode at different scan rates from 10 mV s^{-1} to 100 mV s^{-1}, (d) GCD curves of RHAC/RHCDs electrode at different current densities from 0.5 A g^{-1} to 4 A g^{-1}, (e) recyclability of RHAC/RHCDs electrode (inset: GCD curves of RHAC/RHCDS in 1st cycle and 100th cycle), and (f) Ragone plot of RHAC/RHCDs electrode at current densities from 0.5 A g^{-1} to 4 A g^{-1}.

CHAPTER 5
CONCLUSIONS AND RECOMMENDATIONS

5.1 Conclusions

In this work, the two-in-one synthesis of activated carbon and carbon dots was developed from rice wastes, providing a suitable preparation method. The activated carbon was used as an electrode material for supercapacitors, whereas the carbon dots were used as additives in electrode and electrolyte. CDs act as electro-active species that can reduce series resistance and improve surface wettability resulting in the enhancement of specific capacitance and energy density of supercapacitor. Moreover, rice electrolyte is an alternative electrolyte with a high potential window and high energy density. Based on this work, the developed two-in-one strategy can increase the value of rice waste and possibly pave the way for other biomasses, which can be converted to high-performance energy storage devices for green energy, but not limited to, supercapacitors.

5.2 Recommendations

5.2.1 The H_3PO_4/rice/CDs electrolyte can be further performed to investigate the ionic conductivity.

5.2.2 The rice electrolyte can be further studied for their electrochemical properties using different types of rice such as sticky rice, brown rice, black rice, etc.

5.2.3 The activated carbon and carbon dots from rice wastes can be applied in other applications such as catalysis, adsorption, etc.

REFERENCES

Ahuja, H., Dhapola, P. S., Rahul, Sahoo, N. G., Singh, V., & Singh, P. K. (2020). Ionic liquid (1-hexyl-3-methylimidazolium iodide)-incorporated biopolymer electrolyte for efficient supercapacitor. *High Perform. Polym., 32*(2), 220-225. doi:10.1177/0954008319897763

Arias-Moliz, M. T., Ferrer-Luque, C. M., Espigares-Rodríguez, E., Liébana-Ureña, J., & Espigares-García, M. (2008). Bactericidal activity of phosphoric acid, citric acid, and EDTA solutions against Enterococcus faecalis. *Oral Surg. Oral Med. Oral Pathol. Oral Radiol. Endod., 106*(2), e84-e89. doi:https://doi.org/10.1016/j.tripleo.2008.04.002

Aristov, N., & Habekost, A. (2015). Cyclic Voltammetry - A Versatile Electrochemical Method Investigating Electron Transfer Processes. *World J. Chem. Educ., 3*(5), 115-119. doi:https://doi.org/10.12691/wjce-3-5-2

Ashritha, M. G., & Hareesh, K. (2020). A review on Graphitic Carbon Nitride based binary nanocomposites as supercapacitors. *J. Energy Storage, 32*, 101840. doi:https://doi.org/10.1016/j.est.2020.101840

Atchudan, R., Jebakumar Immanuel Edison, T. N., Shanmugam, M., Perumal, S., Somanathan, T., & Lee, Y. R. (2021). Sustainable synthesis of carbon quantum dots from banana peel waste using hydrothermal process for in vivo bioimaging. *Physica E, 126*, 114417. doi:https://doi.org/10.1016/j.physe.2020.114417

Aziz, S. B., Hamsan, M. H., Abdullah, R. M., & Kadir, M. F. Z. (2019). A Promising Polymer Blend Electrolytes Based on Chitosan: Methyl Cellulose for EDLC Application with High Specific Capacitance and Energy Density. *Molecules, 24*(13). doi:10.3390/molecules24132503

Chen, Z., Zhuo, H., Hu, Y., Zhong, L., Peng, X., Jing, S., Liu, Q., Zhang, X., Liu, C., & Sun, R. (2018). Self-Biotemplate Preparation of Hierarchical Porous Carbon with Rational Mesopore Ratio and High Oxygen Content for an Ultrahigh Energy-Density Supercapacitor. *ACS Sustain. Chem. Eng., 6*(5), 7138-7150. doi:10.1021/acssuschemeng.8b01159

Cheng, Y., Wu, L., Fang, C., Li, T., Chen, J., Yang, M., & Zhang, Q. (2020).
Synthesis of porous carbon materials derived from laminaria japonica via
simple carbonization and activation for supercapacitors. *J. Mater. Res.
Technol., 9*(3), 3261-3271. doi:https://doi.org/10.1016/j.jmrt.2020.01.022

Dao, T. M., & Le Luu, T. (2020). Synthesis of activated carbon from macadamia
nutshells activated by H_2SO_4 and K_2CO_3 for methylene blue removal in water.
Bioresour. Technol., 12, 100583.
doi:https://doi.org/10.1016/j.biteb.2020.100583

Daraghmeh, A., Hussain, S., Saadeddin, I., Servera, L., Xuriguera, E., Cornet, A., &
Cirera, A. (2017). A Study of Carbon Nanofibers and Active Carbon as
Symmetric Supercapacitor in Aqueous Electrolyte: A Comparative Study.
Nanoscale Res. Lett., 12(1), 639-639. doi:10.1186/s11671-017-2415-z

Dhar, A., Kumar, N. S., Khimani, M., Al-Fatesh, A. S., Ibrahim, A. A., Fakeeha, A.
H., Bhadja, P., & Vekariya, R. L. (2020). Naturally occurring neem gum: An
unprecedented green resource for bioelectrochemical flexible energy storage
device. *Int. J. Energ. Res., 44*(2), 913-924. doi:10.1002/er.4949

Ding, C., Deng, Z., Chen, J., & Jin, Y. (2020). One-step microwave synthesis of N,S
co-doped carbon dots from 1,6-hexanediamine dihydrochloride for cell
imaging and ion detection. *Colloid. Surfaces B, 189*, 110838.
doi:https://doi.org/10.1016/j.colsurfb.2020.110838

Eleri, O. E., Azuatalam, K. U., Minde, M. W., Trindade, A. M., Muthuswamy, N.,
Lou, F., & Yu, Z. (2020). Towards high-energy-density supercapacitors via
less-defects activated carbon from sawdust. *Electrochim. Acta, 362*, 137152.
doi:https://doi.org/10.1016/j.electacta.2020.137152

Farhana, N. K., Omar, F. S., Shanti, R., Mahipal, Y. K., Ramesh, S., & Ramesh, K.
(2019). Iota-carrageenan-based polymer electrolyte: impact on ionic
conductivity with incorporation of AmNTFSI ionic liquid for supercapacitor.
Ionics, 25(7), 3321-3329. doi:10.1007/s11581-019-02865-1

Ghann, W., Sharma, V., Kang, H., Karim, F., Richards, B., Mobin, S. M., Uddin, J., Rahman, M. M., Hossain, F., Kabir, H., & Uddin, N. (2019). The synthesis and characterization of carbon dots and their application in dye sensitized solar cell. *Int. J. Hydrog. Ener., 44*(29), 14580-14587. doi:https://doi.org/10.1016/j.ijhydene.2019.04.072

Guo, S., Guo, B., Ma, R., & Zhu, Y. (2020). KOH activation of coal-derived microporous carbons for oxygen reduction and supercapacitors. *RSC Adv., 10*, 15707-15714. doi:10.1039/D0RA01705A

Heidarinejad, Z., Dehghani, M. H., Heidari, M., Javedan, G., Ali, I., & Sillanpää, M. (2020). Methods for preparation and activation of activated carbon: a review. *Environ. Chem. Lett., 18*(2), 393-415. doi:10.1007/s10311-019-00955-0

Heimböckel, R., Hoffmann, F., & Fröba, M. (2019). Insights into the influence of the pore size and surface area of activated carbons on the energy storage of electric double layer capacitors with a new potentially universally applicable capacitor model. *Phys. Chem. Chem. Phys., 21*(6), 3122-3133. doi:10.1039/C8CP06443A

Hsi, H.-C., Horng, R. S., Pan, T.-A., & Lee, S.-K. (2011). Preparation of Activated Carbons from Raw and Biotreated Agricultural Residues for Removal of Volatile Organic Compounds. *J. Air Waste Manage., 61*(5), 543-551. doi:10.3155/1047-3289.61.5.543

Hu, Z., Jiao, X.-Y., & Xu, L. (2020). The N,S co-doped carbon dots with excellent luminescent properties from green tea leaf residue and its sensing of gefitinib. *Microchem. J., 154*, 104588. doi:https://doi.org/10.1016/j.microc.2019.104588

Jaleel, J. A., & Pramod, K. (2018). Artful and multifaceted applications of carbon dot in biomedicine. *J. Control. Release, 269*, 302-321. doi:https://doi.org/10.1016/j.jconrel.2017.11.027

Janewit, W., Worasuwannarak, N., & Pipatmanomai, S. (2008). Product yields and characteristics of rice husk, rice straw and corncob during fast pyrolysis in a drop-tube/fixed-bed reactor. *Songklanakarin J. Sci. Technol., 30*.

Jiang, B., Liang, Y., Yu, X., Yuan, G., Zheng, M., Xiao, Y., Dong, H., Liu, Y., & Hu, H. (2020). Facile synthesis of $FeCO_3$/nitrogen-doped carbon dot composites for lithium-ion battery anodes. *J. Alloy. Compd., 838*, 155508. doi:https://doi.org/10.1016/j.jallcom.2020.155508

Jin, H., Hu, J., Wu, S., Wang, X., Zhang, H., Xu, H., & Lian, K. (2018). Three-dimensional interconnected porous graphitic carbon derived from rice straw for high performance supercapacitors. *J. Power Sources, 384*, 270-277. doi:https://doi.org/10.1016/j.jpowsour.2018.02.089

Jin, L., Zhang, L., Yang, L., Wu, X., Zhang, C., Wei, K., He, L., Han, X., Qiao, H., Asiri, A. M., Alamry, K. A., & Zhang, K. (2020). Orange-red, green, and blue fluorescence carbon dots for white light emitting diodes. *J. Mater. Sci. Technol., 50*, 184-191. doi:https://doi.org/10.1016/j.jmst.2020.03.020

Kasturi, P. R., Ramasamy, H., Meyrick, D., Sung Lee, Y., & Kalai Selvan, R. (2019). Preparation of starch-based porous carbon electrode and biopolymer electrolyte for all solid-state electric double layer capacitor. *J. Colloid Interf. Sci., 554*, 142-156. doi:https://doi.org/10.1016/j.jcis.2019.06.081

Kumar, V. B., Borenstein, A., Markovsky, B., Aurbach, D., Gedanken, A., Talianker, M., & Porat, Z. (2016). Activated Carbon Modified with Carbon Nanodots as Novel Electrode Material for Supercapacitors. *J. Phys. Chem. C, 120*(25), 13406-13413. doi:10.1021/acs.jpcc.6b04045

Kumari, M., & Chaudhary, S. (2020). Modulating the physicochemical and biological properties of carbon dots synthesised from plastic waste for effective sensing of E. coli. *Colloid. Surfaces B, 196*, 111333. doi:https://doi.org/10.1016/j.colsurfb.2020.111333

Le Van, K., & Luong Thi Thu, T. (2019). Preparation of Pore-Size Controllable Activated Carbon from Rice Husk Using Dual Activating Agent and Its Application in Supercapacitor. *J. Chem., 2019*, 4329609. doi:10.1155/2019/4329609

Le Van, K., & Luong Thi, T. T. (2014). Activated carbon derived from rice husk by NaOH activation and its application in supercapacitor. *Pro. Nat. Sci. Mater. Int., 24*(3), 191-198. doi:https://doi.org/10.1016/j.pnsc.2014.05.012

Li, F.-h., Hu, H.-j., Yao, R.-s., Wang, H., & Li, M.-m. (2012). Structure and Saccharification of Rice Straw Pretreated with Microwave-Assisted Dilute Lye. *Ind. Eng. Chem. Res., 51*(17), 6270-6274. doi:10.1021/ie202547w

Li, L., Zhang, N., Zhang, M., Zhang, X., & Zhang, Z. (2019). Flexible $Ti_3C_2T_x$/PEDOT:PSS films with outstanding volumetric capacitance for asymmetric supercapacitors. *Dalton Trans., 48*(5), 1747-1756. doi:https://doi.org/10.1039/C8DT04374D

Liu, D., Zhang, W., & Huang, W. (2019). Effect of removing silica in rice husk for the preparation of activated carbon for supercapacitor applications. *Chin. Chem. Lett., 30*(6), 1315-1319. doi:https://doi.org/10.1016/j.cclet.2019.02.031

Liu, J., Wang, J., Xu, C., Jiang, H., Li, C., Zhang, L., Lin, J., & Shen, Z. X. (2018). Advanced Energy Storage Devices: Basic Principles, Analytical Methods, and Rational Materials Design. *Adv. Sci., 5*(1), 1700322. doi:https://doi.org/10.1002/advs.201700322

Liu, S., Wei, L., & Wang, H. (2020). Review on reliability of supercapacitors in energy storage applications. *Appl. Energ., 278*, 115436. doi:https://doi.org/10.1016/j.apenergy.2020.115436

Long, C., Jiang, Z., Shangguan, J., Qing, T., Zhang, P., & Feng, B. (2021). Applications of carbon dots in environmental pollution control: A review. *Chem. Eng. J., 406*, 126848. doi:https://doi.org/10.1016/j.cej.2020.126848

Lu, W., Cao, X., Hao, L., Zhou, Y., & Wang, Y. (2020). Activated carbon derived from pitaya peel for supercapacitor applications with high capacitance performance. *Mater. Lett., 264*, 127339. doi:https://doi.org/10.1016/j.matlet.2020.127339

Miriyala, N., Ouyang, D., Perrie, Y., Lowry, D., & Kirby, D. J. (2017). Activated carbon as a carrier for amorphous drug delivery: Effect of drug characteristics and carrier wettability. *Eur. J. Pharm. Biopharm., 115*, 197-205. doi:https://doi.org/10.1016/j.ejpb.2017.03.002

Mohideen, M. M., Liu, Y., & Ramakrishna, S. (2020). Recent progress of carbon dots and carbon nanotubes applied in oxygen reduction reaction of fuel cell for transportation. *Appl. Energ., 257*, 114027. doi:https://doi.org/10.1016/j.apenergy.2019.114027

Moreno Araújo Pinheiro Lima, R., & de Oliveira, H. P. (2020). Carbon dots reinforced polypyrrole/ graphene nanoplatelets on flexible eggshell membranes as electrodes of all-solid flexible supercapacitors. *J. Energy Storage, 28*, 101284. doi:https://doi.org/10.1016/j.est.2020.101284

Nair, A., Haponiuk, J. T., Thomas, S., & Gopi, S. (2020). Natural carbon-based quantum dots and their applications in drug delivery: A review. *Biomed. Pharmacother., 132*, 110834. doi:https://doi.org/10.1016/j.biopha.2020.110834

Nam, H., Choi, W., Genuino, D. A., & Capareda, S. C. (2018). Development of rice straw activated carbon and its utilizations. *J. Environ. Chem. Eng., 6*(4), 5221-5229. doi:https://doi.org/10.1016/j.jece.2018.07.045

Prado, M., Silva, E. J. N. L. d., Duque, T. M., Zaia, A. A., Ferraz, C. C. R., Almeida, J. F. A. d., & Gomes, B. P. F. d. A. (2015). Antimicrobial and cytotoxic effects of phosphoric acid solution compared to other root canal irrigants. *J. Appl. Oral Sci., 23*(2), 158-163. doi:10.1590/1678-775720130691

Prasannan, A., & Imae, T. (2013). One-Pot Synthesis of Fluorescent Carbon Dots from Orange Waste Peels. *Ind. Eng. Chem. Res., 52*(44), 15673-15678. doi:10.1021/ie402421s

Rajasekaran, S. J., & Raghavan, V. (2020). Facile synthesis of activated carbon derived from Eucalyptus globulus seed as efficient electrode material for supercapacitors. *Diam. Relat. Mater., 109*, 108038. doi:https://doi.org/10.1016/j.diamond.2020.108038

Rani, U. A., Ng, L. Y., Ng, C. Y., & Mahmoudi, E. (2020). A review of carbon quantum dots and their applications in wastewater treatment. *Adv. Colloid Interfac., 278*, 102124. doi:https://doi.org/10.1016/j.cis.2020.102124

Rashidi, N. A., & Yusup, S. (2020). Recent methodological trends in nitrogen–functionalized activated carbon production towards the gravimetric capacitance: A mini review. *J. Energy Storage, 32*, 101757. doi:https://doi.org/10.1016/j.est.2020.101757

Rezaei, B., Irannejad, N., Ensafi, A. A., & Kazemifard, N. (2019). The impressive effect of eco-friendly carbon dots on improving the performance of dye-sensitized solar cells. *Solar Energy, 182*, 412-419. doi:https://doi.org/10.1016/j.solener.2019.02.072

Saikia, B. K., Benoy, S. M., Bora, M., Tamuly, J., Pandey, M., & Bhattacharya, D. (2020). A brief review on supercapacitor energy storage devices and utilization of natural carbon resources as their electrode materials. *Fuel, 282*, 118796. doi:https://doi.org/10.1016/j.fuel.2020.118796

Santos, T. M., de Jesus, F. A., da Silva, G. F., & Pontes, L. A. M. (2020). Synthesis of activated carbon from oleifera moringa for removal of oils and greases from the produced water. *Environ. Nanotechnol. Monit. Manag., 14*, 100357. doi:https://doi.org/10.1016/j.enmm.2020.100357

Senthilkumar, S. T., Selvan, R. K., & Melo, J. S. (2013). Redox additive/active electrolytes: a novel approach to enhance the performance of supercapacitors. *J. Mater. Chem. A, 1*(40), 12386-12394. doi:10.1039/C3TA11959A

Sesuk, T., Tammawat, P., Jivaganont, P., Somton, K., Limthongkul, P., & Kobsiriphat, W. (2019). Activated carbon derived from coconut coir pith as high performance supercapacitor electrode material. *J. Energy Storage, 25*, 100910. doi:https://doi.org/10.1016/j.est.2019.100910

Shao, J., Zhou, X., Liu, Q., Zou, R., Li, W., Yang, J., & Hu, J. (2015). Mechanism analysis of the capacitance contributions and ultralong cycling-stability of the isomorphous MnO_2@MnO_2 core/shell nanostructures for supercapacitors. *J. Mater. Chem. A, 3*(11), 6168-6176. doi:https://doi.org/10.1039/C4TA06793B

Sudhan, N., Subramani, K., Karnan, M., Ilayaraja, N., & Sathish, M. (2017). Biomass-Derived Activated Porous Carbon from Rice Straw for a High-Energy Symmetric Supercapacitor in Aqueous and Non-aqueous Electrolytes. *Energ. Fuel., 31*(1), 977-985. doi:10.1021/acs.energyfuels.6b01829

Supchocksoonthorn, P., Thongsai, N., Wei, W., Gopalan, P., & Paoprasert, P. (2021). Highly sensitive and stable sensor for the detection of capsaicin using electrocatalytic carbon dots grafted onto indium tin oxide. *Sens. Actuators, B, 329*, 129160. doi:https://doi.org/10.1016/j.snb.2020.129160

Teo, E. Y. L., Muniandy, L., Ng, E.-P., Adam, F., Mohamed, A. R., Jose, R., & Chong, K. F. (2016). High surface area activated carbon from rice husk as a high performance supercapacitor electrode. *Electrochimica Acta, 192*, 110-119. doi:https://doi.org/10.1016/j.electacta.2016.01.140

Thongsai, N., Tanawannapong, N., Praneerad, J., Kladsomboon, S., Jaiyong, P., & Paoprasert, P. (2019). Real-time detection of alcohol vapors and volatile organic compounds via optical electronic nose using carbon dots prepared from rice husk and density functional theory calculation. *Colloid. Surfaces A, 560*, 278-287. doi:https://doi.org/10.1016/j.colsurfa.2018.09.077

Ukkakimapan, P., Sattayarut, V., Wanchaem, T., Yordsri, V., Phonyiem, M., Ichikawa, S., Obata, M., Fujishige, M., Takeuchi, K., Wongwiriyapan, W., & Endo, M. (2020). Preparation of activated carbon via acidic dehydration of durian husk for supercapacitor applications. *Diam. Relat. Mater., 107*, 107906. doi:https://doi.org/10.1016/j.diamond.2020.107906

Usha Rani, M., Nanaji, K., Rao, T. N., & Deshpande, A. S. (2020). Corn husk derived activated carbon with enhanced electrochemical performance for high-voltage supercapacitors. *J. Power Sources, 471*, 228387. doi:https://doi.org/10.1016/j.jpowsour.2020.228387

Vinodh, R., Gopi, C. V. V. M., Kummara, V. G. R., Atchudan, R., Ahamad, T., Sambasivam, S., Yi, M., Obaidat, I. M., & Kim, H.-J. (2020). A review on porous carbon electrode material derived from hypercross-linked polymers for supercapacitor applications. *J. Energy Storage, 32*, 101831. doi:https://doi.org/10.1016/j.est.2020.101831

Wang, L., & Zhou, H. S. (2014). Green Synthesis of Luminescent Nitrogen-Doped Carbon Dots from Milk and Its Imaging Application. *Anal. Chem., 86*(18), 8902-8905. doi:10.1021/ac502646x

Wang, S., Wang, H., Zhang, R., Zhao, L., Wu, X., Xie, H., Zhang, J., & Sun, H. (2018). Egg yolk-derived carbon: Achieving excellent fluorescent carbon dots and high performance lithium-ion batteries. *J. Alloy. Compd., 746*, 567-575. doi:https://doi.org/10.1016/j.jallcom.2018.02.293

Wang, Y., Sun, J., He, B., & Feng, M. (2020). Synthesis and modification of biomass derived carbon dots in ionic liquids and their application: a mini review. *Green Chem. Eng.* doi:https://doi.org/10.1016/j.gce.2020.09.010

Wen, Q.-L., Pu, Z.-F., Yang, Y.-J., Wang, J., Wu, B.-C., Hu, Y.-L., Liu, P., Ling, J., & Cao, Q. (2020). Hyaluronic acid as a material for the synthesis of fluorescent carbon dots and its application for selective detection of Fe^{3+} ion and folic acid. *Microchem. J., 159*, 105364. doi:https://doi.org/10.1016/j.microc.2020.105364

Xia, T., Sun, E., Tang, W., Huang, H., Wu, G., & Jin, X. (2018). Structural and Thermal Stability Changes of Rice Straw Fibers during Anaerobic Digestion. *Bioresources*. Retrieved from https://ojs.cnr.ncsu.edu/index.php/BioRes/article/view/13507

Xu, H., Gao, B., Cao, H., Chen, X., Yu, L., Wu, K., Sun, L., Peng, X., & Fu, J. (2014). Nanoporous Activated Carbon Derived from Rice Husk for High Performance Supercapacitor. *J. Nanomater., 2014*, 714010. doi:10.1155/2014/714010

Yakaboylu, G. A., Jiang, C., Yumak, T., Zondlo, J. W., Wang, J., & Sabolsky, E. M. (2021). Engineered hierarchical porous carbons for supercapacitor applications through chemical pretreatment and activation of biomass precursors. *Renew. Energ., 163*, 276-287. doi:https://doi.org/10.1016/j.renene.2020.08.092

Yu, J., Joo, S., Sim, T., Hong, S., Kim, O., & Kang, J. (2020). Post-KOH activation of nitrogen-containing porous carbon with ordering mesostructure synthesized through a self-assembly. *Chem. Phys. Lett., 739*, 137028. doi:https://doi.org/10.1016/j.cplett.2019.137028

Zainuddin, N. K., Rasali, N. M. J., Mazuki, N. F., Saadiah, M. A., & Samsudin, A. S. (2020). Investigation on favourable ionic conduction based on CMC-K carrageenan proton conducting hybrid solid bio-polymer electrolytes for applications in EDLC. *Int. J. Hydrogen Energ., 45*(15), 8727-8741. doi:https://doi.org/10.1016/j.ijhydene.2020.01.038

Zhang, S., Shi, X., Chen, X., Zhang, D., Liu, X., Zhang, Z., Chu, P. K., Tang, T., & Mijowska, E. (2019). Large-Scale and Low-Cost Motivation of Nitrogen-Doped Commercial Activated Carbon for High-Energy-Density Supercapacitor. *ACS Appl. Energ. Mater., 2*(6), 4234-4243. doi:10.1021/acsaem.9b00481

Zhao, K., Zheng, X., Zhang, H., Xu, M., Wang, S., Yang, Q., & Xiong, C. (2019). Multi-color fluorescent carbon dots with single wavelength excitation for white light-emitting diodes. *J. Alloy. Compd., 793*, 613-619. doi:https://doi.org/10.1016/j.jallcom.2019.04.146

Zhong, C., Deng, Y., Hu, W., Qiao, J., Zhang, L., & Zhang, J. (2015). A review of electrolyte materials and compositions for electrochemical supercapacitors. *Chem. Soc. Rev., 44*(21), 7484-7539. doi:10.1039/C5CS00303B

Zhou, D., Li, D., Li, A., Qi, M., Cui, D., Wang, H., & Wei, H. (2020). Activated carbons prepared via reflux-microwave-assisted activation approach with high adsorption capability for methylene blue. *J. Environ. Chem. Eng.*, 104671. doi:https://doi.org/10.1016/j.jece.2020.104671

Zhou, G., Yin, J., Sun, Z., Gao, X., Zhu, F., Zhao, P., Li, R., & Xu, J. (2020). An ultrasonic-assisted synthesis of rice-straw-based porous carbon with high performance symmetric supercapacitors. *RSC Adv., 10*(6), 3246-3255. doi:10.1039/C9RA08537H

Zhu, M., Yu, L., He, S., Hong, H., Liu, J., Gan, L., & Long, M. (2019). Highly Efficient and Stable Cellulose-Based Ion Gel Polymer Electrolyte for Solid-State Supercapacitors. *ACS Appl. Ener. Mater., 2*(8), 5992-6001. doi:10.1021/acsaem.9b01109

APPENDIX

Specific surface area, pore volume, and pore size of rice straw activated carbon
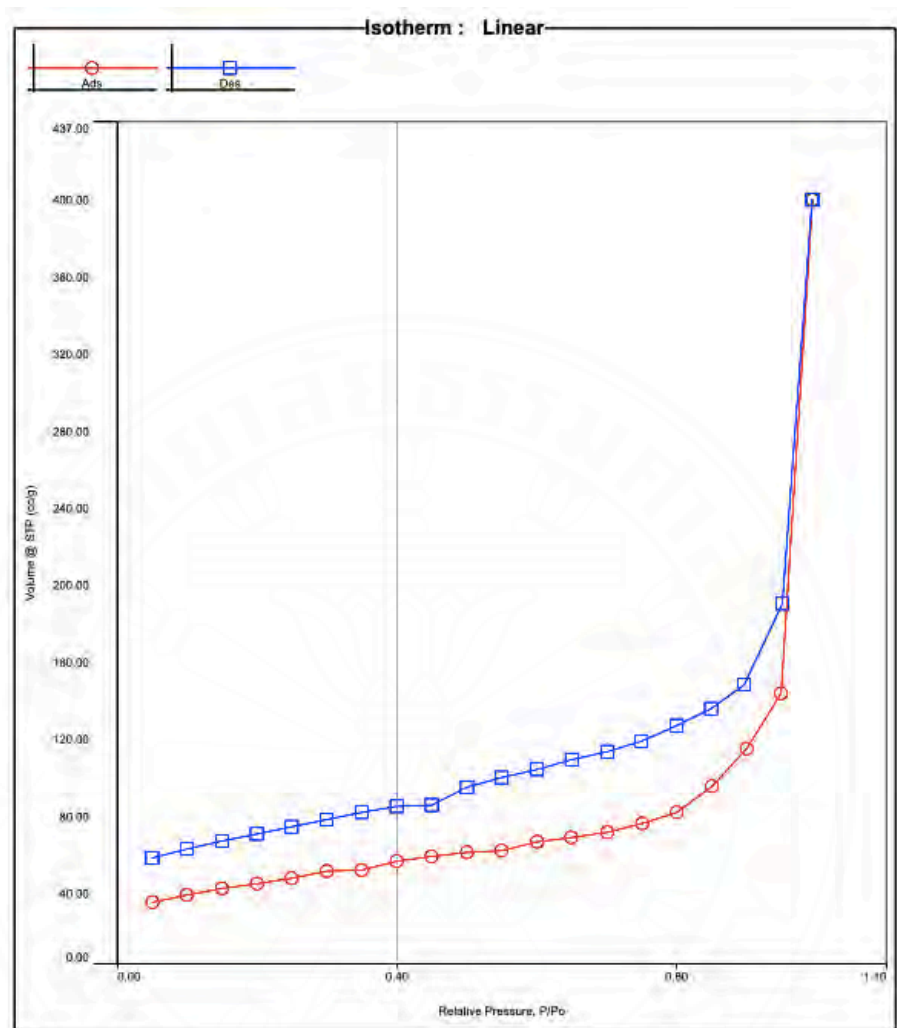
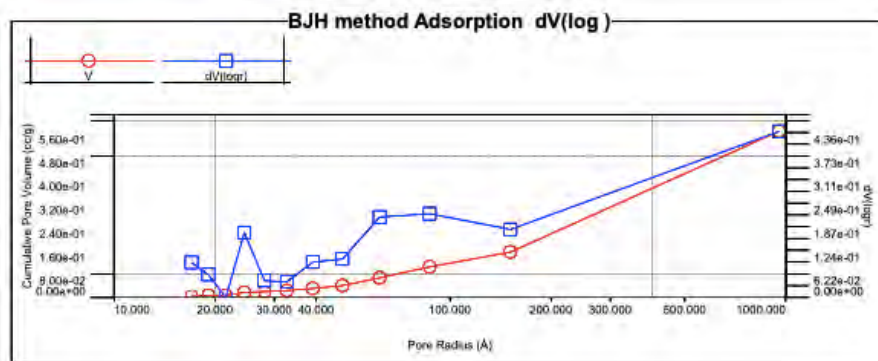*Figure A1* Nitrogen adsorption-desorption isotherm of RSAC1
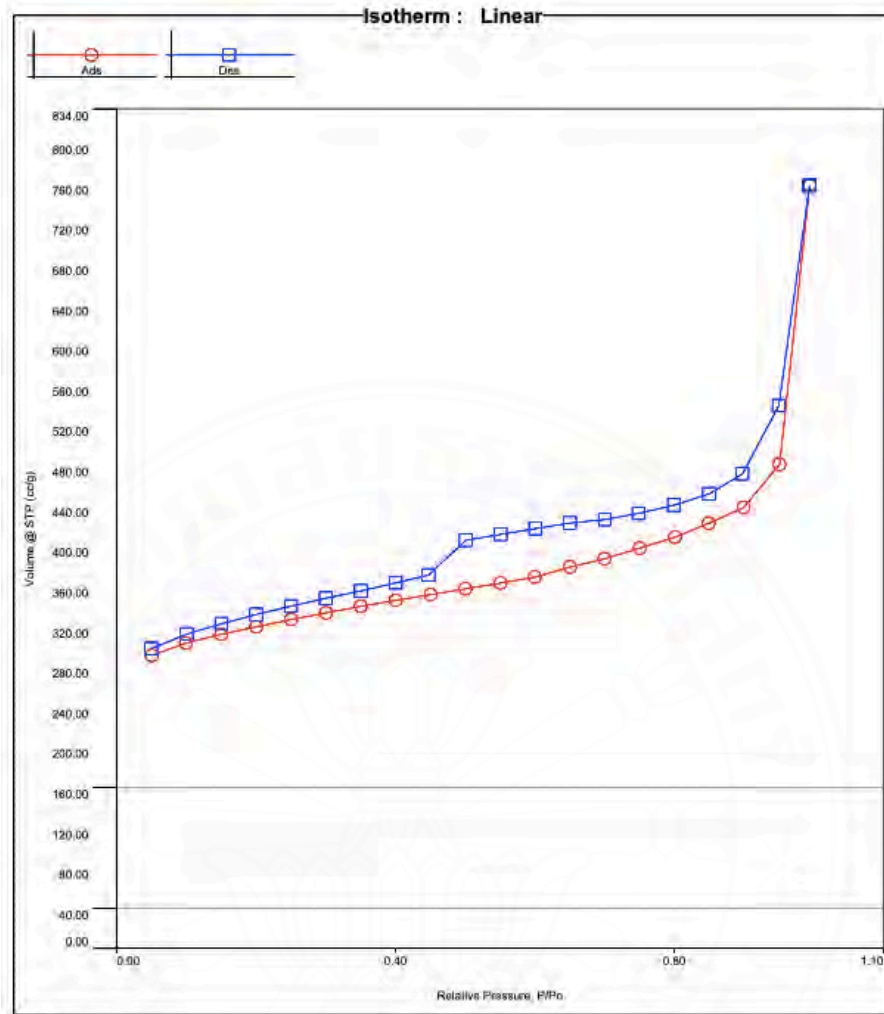

Figure A2 BJH plot of RSAC1

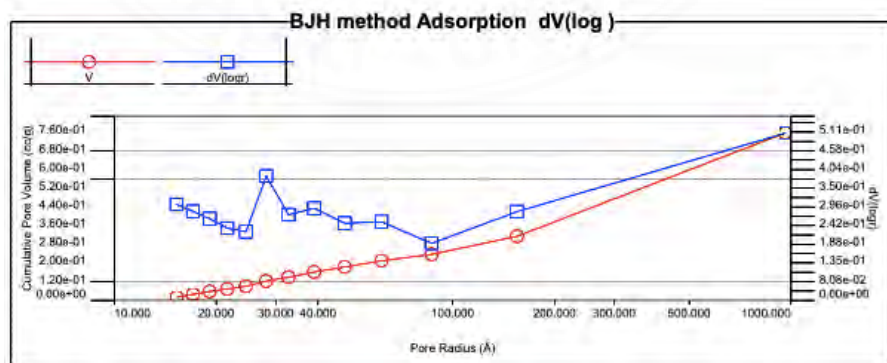*Figure A3* Nitrogen adsorption-desorption isotherm of RSAC2
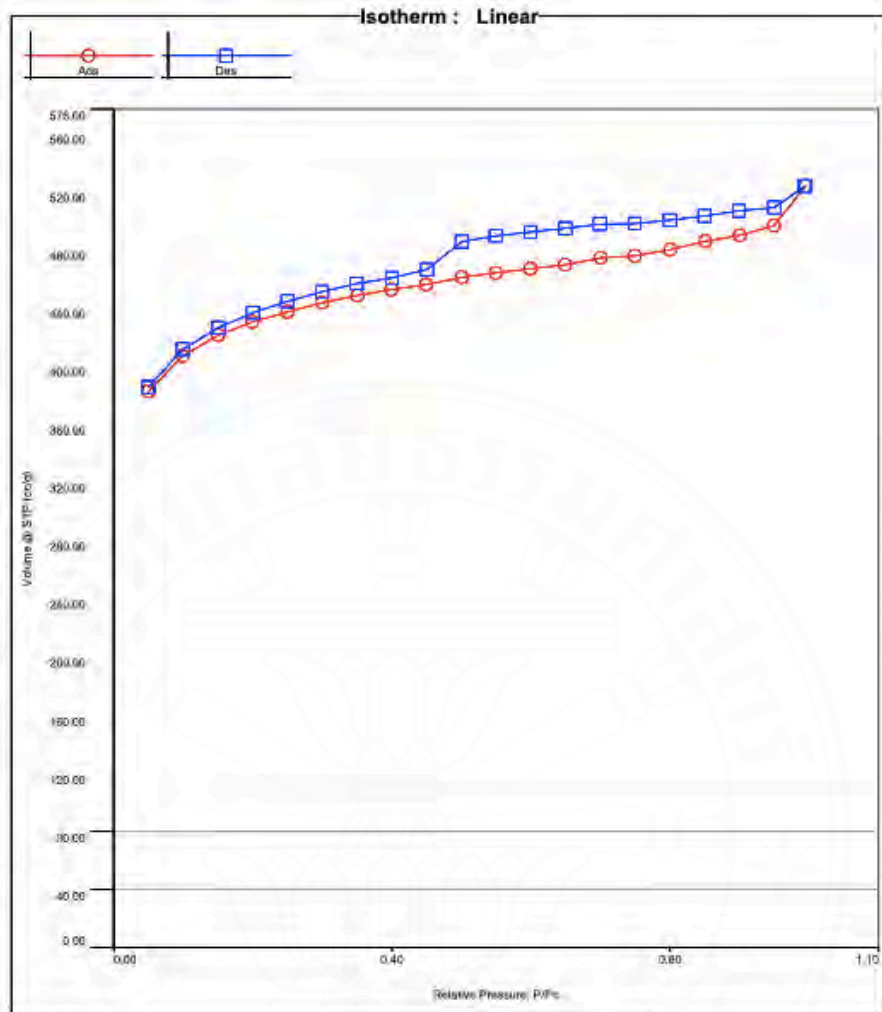

Figure A4 BJH plot of RSAC2

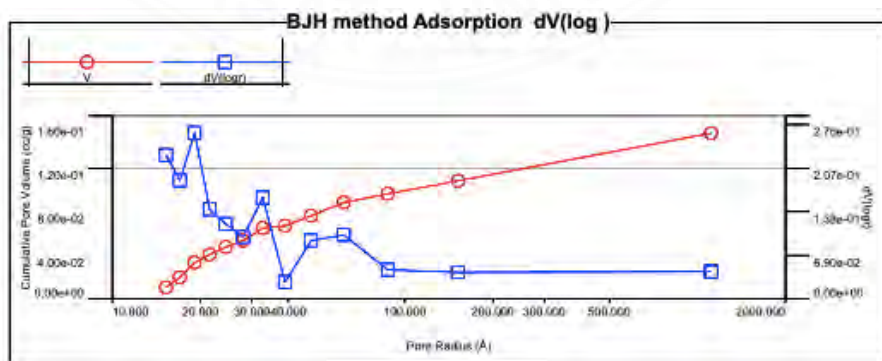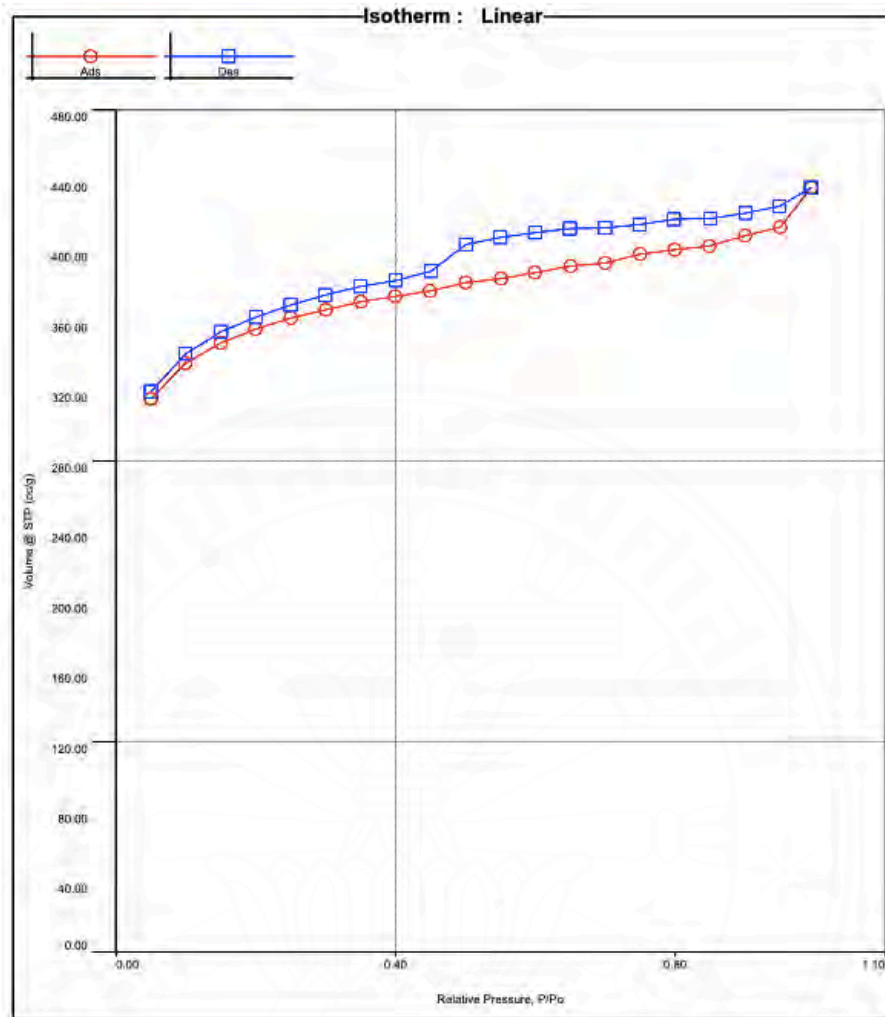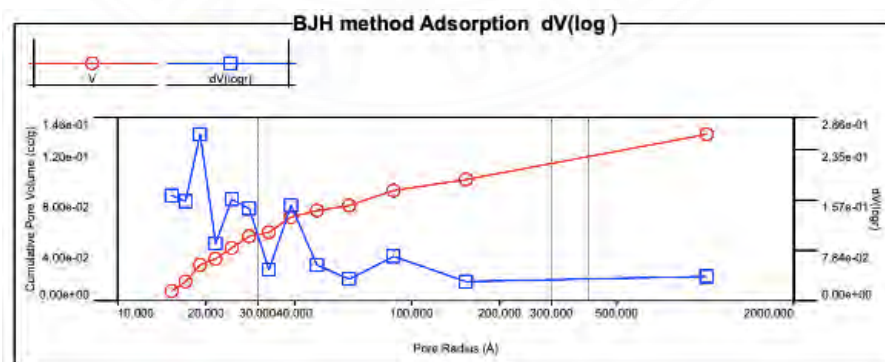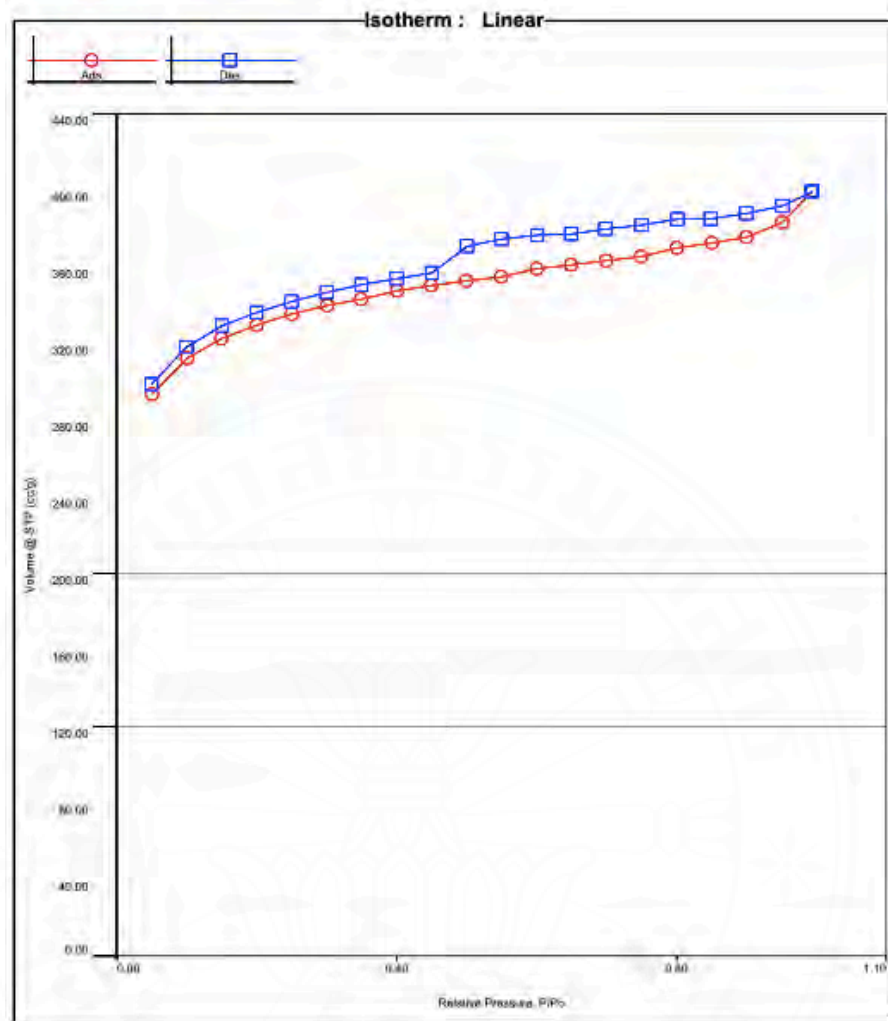*Figure A5* Nitrogen adsorption-desorption isotherm of RSAC3

Figure A6 BJH plot of RSAC3

Figure A7 Nitrogen adsorption-desorption isotherm of RSAC4

Figure A8 BJH plot of RSAC4

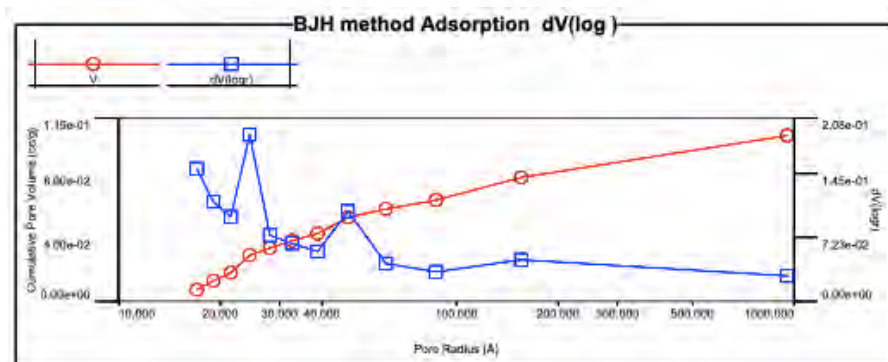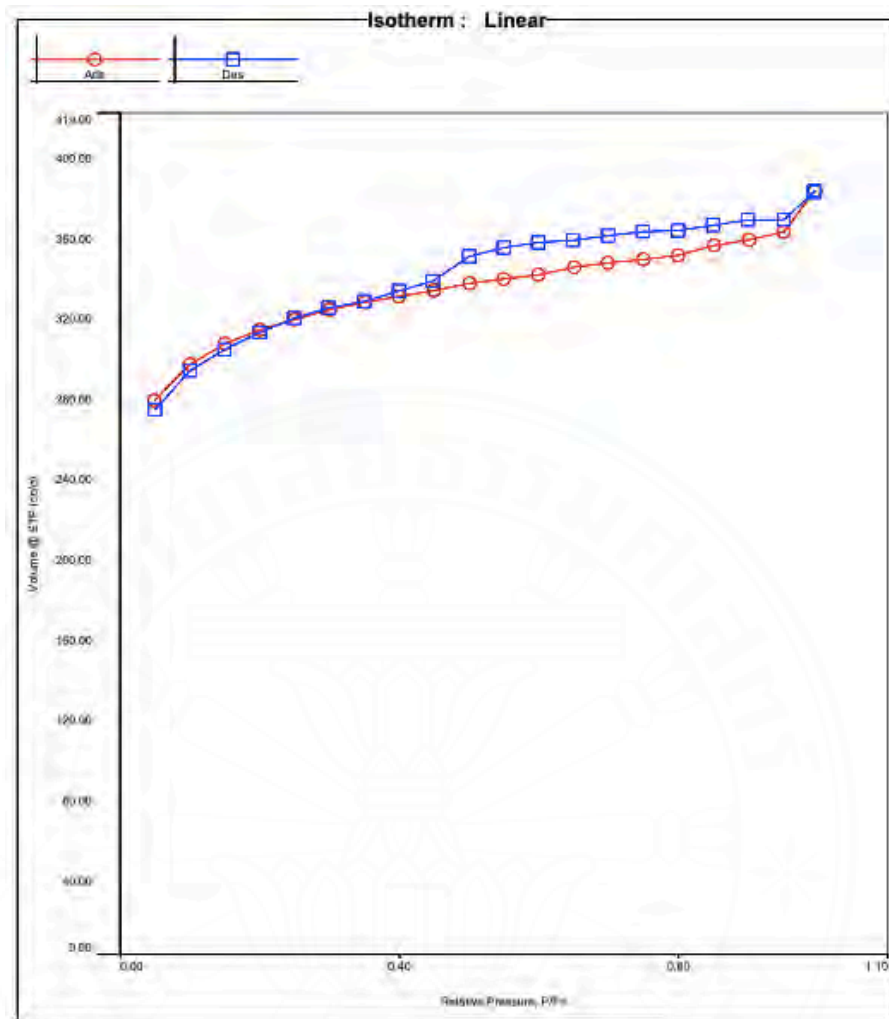*Figure A9* Nitrogen adsorption-desorption isotherm of RSAC5

Figure A10 BJH plot of RSAC5

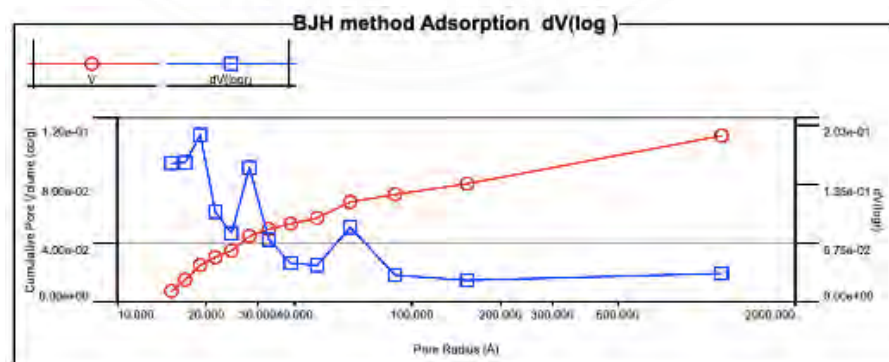*Figure A11* Nitrogen adsorption-desorption isotherm of RSAC6

Figure A12 BJH plot of RSAC6

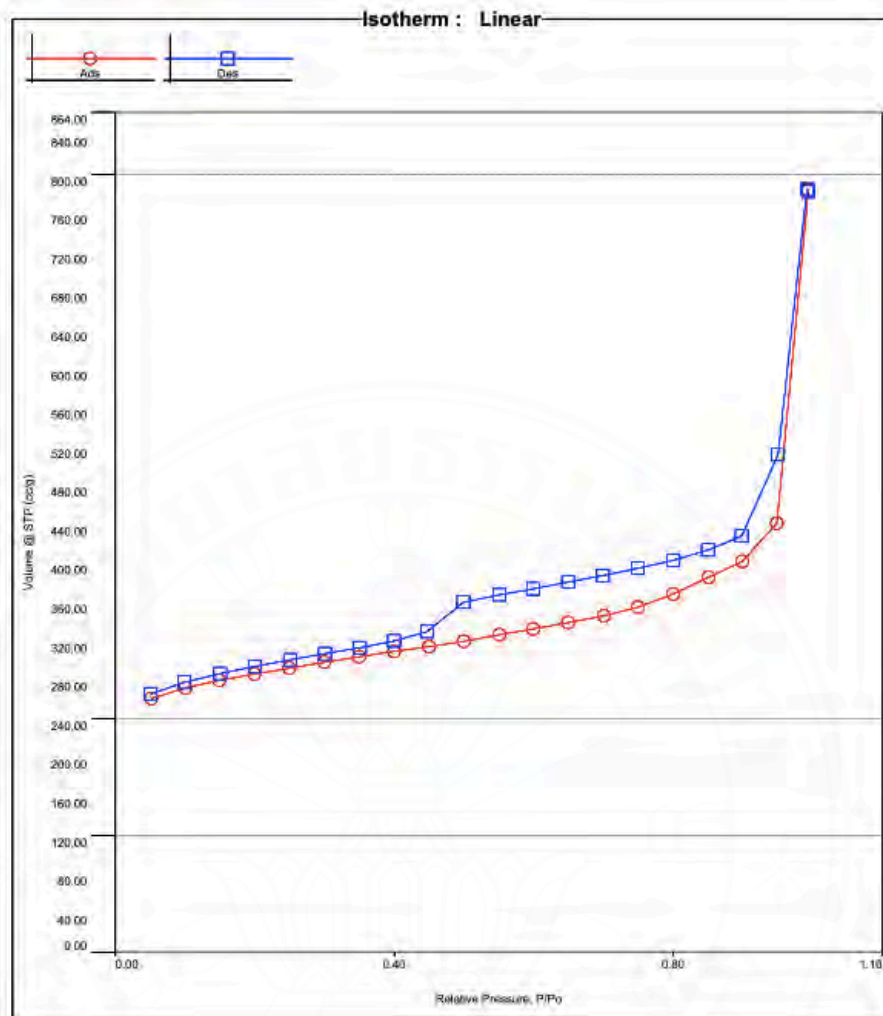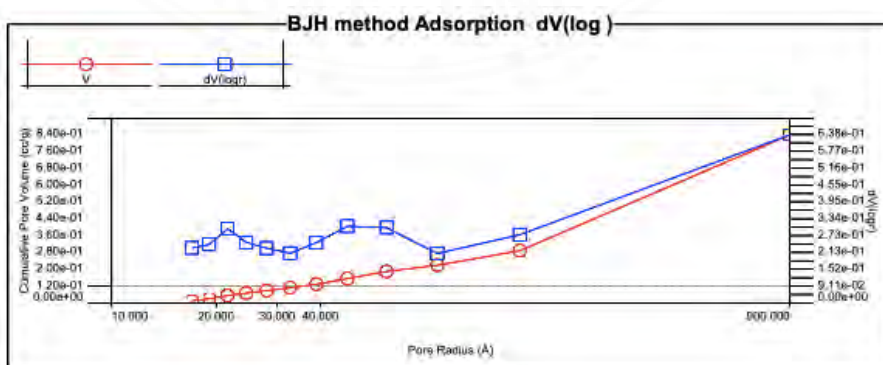*Figure A13* Nitrogen adsorption-desorption isotherm of RSAC7

Figure A14 BJH plot of RSAC7

BIOGRAPHY

Name	Mr Thanapat Jorn-am
Date of Birth	July 6, 1996
Educational Attainment	Academic Year 2018: Bachelor of Science (Chemistry), Thammasat University, Thailand
Scholarship	Year 2019-2020: Scholarship for Talent Student to Study Graduate Program in Faculty of Science and Technology Thammasat University, Contract No. TB 22/2019.

Publications

Thanapat Jorn-am, Peerasak Paoprasert. Two-in-One Synthesis of Carbon Dots and
Activated Carbon from Rice Husk for Supercapacitor with Improved
Performance. Thai Society for Biotechnology International Conference
Proceeding, 2021, 400-404.

Petty Patents

Jirada Singkhonrat and Thanapat Jorn-am. A Cap with the Solar System, 2019, No.
1903003244.

Peerasak Paoprasert, Janjira Praneerad, Thitarat Prathumsuwan, Kulpriya
Phetcharee, Thanapat Jorn-am, and Monthakarn Supjaroenpisan.
Preparation of Nanocarbon Particle from Sugar for Sunscreen, Antioxidant,
and Metal Ion Absorption, 2019, No. 1903002612.

Activities and Awards	2021: Best Oral Presentation Award from Thai Society for Biotechnology International Conference Online (TSB Online)

2020: Outstanding Poster Presentation Award from Pure and Applied Chemistry International Conference 2020 (PACCAN 2020)

2019: Best of Senior Project Oral Presentation Award from Department of Chemistry, Faculty of Science and Technology, Thammasat University

2019: Best of Poster Presentation Award from Department of Chemistry, Faculty of Science and Technology, Thammasat University

2018: 1st Runner Up Award and Outstanding Award from ISC Pitching Challenge 2018

Work Experiences   2019: Teacher Assistant of Fundamental Chemistry Laboratory and General Organic Chemistry Laboratory at Faculty of Science and Technology, Thammasat University, Thailand